INTERNATIONAL JOURNAL FOR NUMERICAL METHODS IN ENGINEERING

Int. J. Numer. Meth. Engng 2006; **00**:1–51 *Prepared using* nmeauth.cls *[Version: 2002/09/18 v2.02]*

A general discontinuous Galerkin method for finite hyperelasticity. Formulation and numerical applications.

L. Noels[1,2,†], R. Radovitzky[1,*]

[1] *Massachusetts Institute of Technology, Department of Aeronautics and Astronautics*

77 Massachusetts Ave, Cambridge, MA 02139-4307

[2] *University of Liège, LTAS-Milieux Continus & Thermomécanique*

Chemin des Chevreuils 1, B-4000 Liège, Belgium

SUMMARY

A discontinuous Galerkin formulation of the Boundary Value Problem of finite-deformation elasticity is presented. The primary purpose is to establish a discontinuous Galerkin framework for large deformations of solids in the context of statics and simple material behavior with a view toward further developments involving behavior or models where the DG concept can show its superiority compared to the continuous formulation. The method is based on a general Hu-Washizu-de Veubeke functional allowing for displacement and stress discontinuities in the domain interior. It is shown that this approach naturally leads to the formulation of average stress fluxes at interelement boundaries in a finite element implementation. The consistency and linearized stability of the method in the non-linear range as well as its convergence rate are proven. An implementation in three dimensions is developed, showing that the proposed method can be integrated into conventional finite element

*Correspondence to: Tel: +1-617-252-1518, Fax: +1-617-253-0361, E-mail: rapa@mit.edu

†Research Fellow at the Belgian National Fund for Scientific Research (FNRS)

Received

Revised

codes in a straightforward manner. In order to demonstrate the versatility, accuracy and robustness of the method examples of application and convergence studies in three dimensions are provided.

KEY WORDS: Discontinuous Galerkin method; large deformation of solids; finite-element method

1. INTRODUCTION

Discontinuous Galerkin methods constitute a generalization of weak formulations allowing for discontinuities of the problem unknowns in the interior of the problem domain. This is accomplished by restricting the integration by parts to subdomains, which naturally leads to boundary integral terms on the subdomain interfaces involving jump discontinuities. Clearly, the role of these terms is to enforce the consistency and the continuity of the problem unknowns in a weakly manner, where appropriate. In the context of finite element formulations of elliptic problems, jump-discontinuities are allowed across element boundaries. The main appeal of discontinuous Galerkin methods lies in their ability to represent physical discontinuities present in the problem solution in a natural way. One of the obvious compromises is the explosion in the number of degrees of freedom of the discrete problem without an increase of the order of accuracy in smooth regions of the solution. However, this disadvantage can be significantly alleviated since the method is amenable to efficient parallel implementations. A common problem encountered in the formulation of discontinuous Galerkin methods is non-uniqueness of the discrete problem solution and the appearance of spurious energy at element interfaces, a problem that was identified in the early contribution by Nitsche [1], who introduced a stabilization term on the boundary to enforce weakly the homogeneous Dirichlet

boundary condition. Stabilization is now frequently achieved through a quadratic boundary term. Another one of the earliest papers in this area corresponds to Reed and Hill [2] who proposed a discontinuous Galerkin method for neutron transport problems.

In recent years, a significant number of results has been obtained in the area of discontinuous Galerkin methods applied to hyperbolic problems. A recent report by Cockburn [3] discusses at length the main results, see also [4]. Discontinuous Galerkin methods appear to be efficient with trial and weighting functions of high polynomial order k. For the linear one dimensional hyperbolic equation the L^2-stability is proved and the L^2-norm error has a convergence rate of at least $k + \frac{1}{2}$ in the mesh size. In the non-linear case, only L^1-stability can be demonstrated, and the convergence-rate cannot be achieved. To achieve conditional stability of the time integration by an explicit Range-Kutta method *slope limiters* were introduced *e.g.* [5]. More recent results include a space-time discontinuous Galerkin method for hyperbolic equations, using slope limiters to control numerical oscillations [6].

For non-linear convection/diffusion problems (compressible Navier-Stokes equations), Bassi and Rebay [7] proposed to consider the conservative variables as well as their gradients as independent unknowns as a means of obtaining a lumped mass matrix, which enables efficient parallel implementations. Cockburn and Shu [8] proposed a generalization of this method and demonstrated L^2-stability both for linear and non-linear scalar equations of convection/diffusion problems. They also showed that for linear problems the convergence rate of the error is between k and $k + 1$ and that the L^2-stability holds in multidimensions. Another finding in that work was that non-linear stability of the Range-Kutta time integration (explicit two-stage in the work of Bassi and Rebay [7]) can be reached without the use of slope limiters.

In the context of elliptic problems, Brezzi *et al* [9] proposed a discontinuous Galerkin method to solve the scalar Poisson equation. They presented a rigorous formalism based on the work of Bassi and Rebay [7] which leads to specific forms of stabilization terms. Both the primary unknown and its gradients were initially considered independent. But, owing to the linearity of the problem, they reduced the system to a single equation on the primary unknown, whereas Bassi and Rebay [7] used a staggered mixed method. Kim [10] presented a mixed discontinuous Galerkin formalism for a non-linear elliptic scalar equation appearing in the computation of stationary magnetic fields. Lew *et al* [11] generalized the method of Brezzi *et al* to linear elasticity. Their formulation derives from a discrete variational principle applied to the Hellinger-Reissner functional. They demonstrated the L^2-stability of the method and derived its convergence rate. It bears emphasis that in these references the formulation is provided without numerical implementation or verification examples. There have been other recent contributions in the area of discontinuous Galerkin methods applied to solid mechanics. In most cases, attention has been restricted to linear elasticity problems. Hansbo and Larson [12] used a discontinuous Galerkin method to avoid locking in near-incompressible elasticity. Engel *et al* [13] proposed a discontinuous Galerkin approach for fourth-order elliptic problems where conventional approximations with C^0 interelement continuity is adopted and the C^1 compatibility requirement is enforced weakly by the discontinuous Galerkin formulation. They included an implementation and examples of application to beam, plate and simple micropolar continuum problems.

Time discontinuous Galerkin approaches have been applied to elastodynamics in combination or not with a space-discontinuous Galerkin method. Hang and Constanzo [14, 15] proposed a space-time discontinuous Galerkin formulation for linear-elasticity where stress

discontinuities were considered through jumps in the material properties. This discontinuity can be propagated through the system assuming that at each time step the discontinuity is located at the element interfaces. Bonelli *et al* [16] and Chien *et al* [17] proposed to solve transient elastodynamics problems by using a continuous method in space and a discontinuous Galerkin method in time. In such method, both displacements and velocities are independent unknowns. Alberty and Cartensen [18] pointed out the advantage of discontinuous Galerkin time integration in the treatment of plasticity.

The primary purpose of this work is to establish a discontinuous Galerkin framework for large deformations of solids in the context of statics and simple material behavior with a view toward further developments involving material behavior or models where the DG concept can show its superiority compared to the continuous formulation. Examples include: problems in which actual discontinuities may appear in the solution such as fracture and problems involving theories requiring higher-order continuity such as gradient theories of plasticity, in which the DG approach can provide a rigorous way of weakly enforcing this continuity requirement. For example, Mergheim *et al* [19] proposed to use the space-discontinuous Galerkin method as a means of enforcing weakly the continuity between the elements before the onset of failure. As pointed out by Zienkiewicz *et al* [20], the discontinuities are appropriately described if they are coincident with the element interfaces).

To this end, a discontinuous Galerkin formulation for large deformations of elastic bodies is proposed. The method is applicable to a wide class of hyperelastic material models. An extension of the three-field Hu-Washizu-de Veubeke functional to large deformations allowing for discontinuities of displacements and stresses is taken as a starting point for developing the method. The resulting weak form naturally leads to the formulation of average stress fluxes

at interelement boundaries in a finite element implementation. It is shown how the equations can be reduced to a one-field formulation, thus simplifying the numerical implementation. The consistency and linearized stability of the method in the non-linear range as well as its convergence rate are proven. An implementation in three dimensions is developed, showing that the proposed method can be integrated into conventional finite element codes without significant effort. In order to demonstrate the versatility, accuracy and robustness of the method examples of application and convergence studies in three dimensions are provided. We emphasize the point that we want to develop a framework for discontinuous Galerkin method in non-linear mechanics and therefore just want to demonstrate that the method does not lead to a loss of accuracy for the numerical examples studied. It is not our purpose to demonstrate that the method works better than continuous method. In future work we will use the developed formulation in specific problems such as failure for which continuous method have limitations.

In section 2 the problem statement and numerical formulation are presented. Section 3 provides details of the implementation in terms of interface elements. This implementation requires only a few modifications to an existing finite element code. Finally in section 4 we present examples of application in three dimensions providing numerical evidence of the established properties of the method and demonstrating the accuracy and robustness of the method in the presence of large deformations.

2. CONTINUUM PROBLEM STATEMENT AND DISCONTINUOUS GALERKIN FORMULATION

We consider the boundary value problem of large static deformations of elastic bodies in equilibrium. The continuum problem is governed by the following equations stated in material form [21]:

$$\nabla_0 \mathbf{P} + \rho_0 \mathbf{B} = \mathbf{0} \text{ in } B_0 \tag{1}$$

$$\boldsymbol{\varphi} = \bar{\boldsymbol{\varphi}} \text{ on } \partial_D B_0 \tag{2}$$

$$\mathbf{P} \cdot \mathbf{N} = \bar{\mathbf{T}} \text{ on } \partial_N B_0 \tag{3}$$

In these expressions, $B_0 \subset \mathbb{R}^3$ is the region of space occupied by the body in its reference configuration, $\mathbf{P}$ is the first Piola-Kirchhoff stress tensor, $\rho_0 \mathbf{B}$ are the body forces per unit reference volume, ∇_0 is the gradient operator with respect to the reference frame, $\boldsymbol{\varphi}$ is the deformation mapping describing the deformation of material particles, $\mathbf{N}$ is the unit surface normal in the reference configuration and $\bar{\boldsymbol{\varphi}}$ and $\bar{\mathbf{T}}$ are the boundary conditions applied on the displacement $\partial_D B_0$ and traction $\partial_N B_0$ parts of the boundary, respectively. Also, $\partial B_0 = \partial_D B_0 \cup \partial_N B_0$ and $\partial_D B_0 \cap \partial_N B_0 = \emptyset$.

A general class of hyperelastic material models is considered for which the stresses can be derived from an assumed strain energy density function $W = W(\mathbf{F})$ by direct differentiation:

$$\mathbf{P} = \frac{\partial W}{\partial \mathbf{F}} \tag{4}$$

In these expressions, $\mathbf{F} = \boldsymbol{\nabla}_0 \boldsymbol{\varphi}$ are the deformation gradients. Material frame indifference restricts the dependence of W on $\mathbf{F}$ as $W = W(\mathbf{C})$, where $\mathbf{C} = \mathbf{F}^T \mathbf{F}$ is the right Cauchy-Green deformation tensor.

A standard exercise shows that equations (1)-(4) constitute the Euler-Lagrange equations corresponding to the three-field Hu-Washizu-de Veubeke [22, 23, 24] energy functional (regarding denomination, see also [25]) $I(\boldsymbol{\varphi},\mathbf{F},\mathbf{P}) : \mathrm{H}^1(B_0) \times \left[\mathrm{H}^0(B_0)\right]^2 \times \left[\mathrm{H}^0(B_0)\right]^2 \to \mathbb{R}$

$$I(\boldsymbol{\varphi},\mathbf{F},\mathbf{P}) = \int_{B_0} \left[W(\mathbf{F}) - \rho_0 \mathbf{B}\cdot\boldsymbol{\varphi} + \mathbf{P} : (\boldsymbol{\nabla}_0\boldsymbol{\varphi} - \mathbf{F})\right] dV_0 - \int_{\partial_D B_0} (\boldsymbol{\varphi} - \bar{\boldsymbol{\varphi}})\cdot\mathbf{P}\cdot\mathbf{N} dS_0 - \int_{\partial_N B_0} \bar{\mathbf{T}}\cdot\boldsymbol{\varphi} dS_0 \quad (5)$$

where $\mathrm{H}^1(B_0)$, $\left[\mathrm{H}^0(B_0)\right]^2$ are the appropriate Sobolev spaces. The energy functional (5) is taken as a basis for numerical discretization. Toward this end, the reference configuration B_0 is approximated by a subdivision (mesh) B_{0h} as shown schematically in Figure 1 such that :

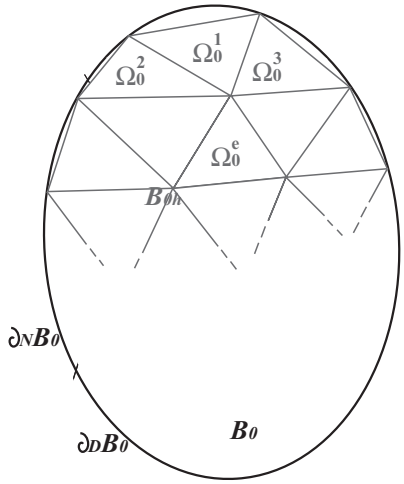

Figure 1. Schematic of the discrete representation of elastic domain B_0 as a subdivision B_{0h}

$$\begin{aligned} B_0 \sim B_{0h} &= \bigcup_{e=1}^{E} \Omega_0^e \\ \bar{\Omega}_0^e \bigcap_{\forall e \neq e'} \bar{\Omega}_0^{e'} &= \emptyset \end{aligned} \quad (6)$$

where $\bar{\Omega}_0^e$ represents the interior of subdomain Ω_0^e. It is assumed that B_{0h} satisfies the necessary admissibility and Lipschitz continuity conditions, [26]. A finite-dimensional piecewise

polynomial approximation $\boldsymbol{\varphi}_h, \mathbf{F}_h, \mathbf{P}_h$ of the fields $\boldsymbol{\varphi}, \mathbf{F}$ and $\mathbf{P}$ is defined on B_{0h} by introducing the following spaces:

$$\mathrm{X}_{\mathrm{h}}^{k} = \left\{ \boldsymbol{\varphi}_{\mathrm{h}} \in \mathrm{L}^2\left(B_{0h}\right) |_{\left[\boldsymbol{\varphi}_{\mathrm{h}}|_{\Omega_0^e} \in \mathbb{P}^k\left(\Omega_0^e\right) \quad \forall \Omega_0^e \in B_{0h}\right]} \right\} \tag{7}$$

$$\mathrm{E}_{\mathrm{h}}^{k} = \left\{ \mathbf{F}_{\mathrm{h}} \in \left[\mathrm{L}^2\left(B_{0h}\right)\right]^2 |_{\left[\mathbf{F}_{\mathrm{h}}|_{\Omega_0^e} \in \mathbb{P}^k\left(\Omega_0^e\right)^2 \quad \forall \Omega_0^e \in B_{0h}\right]} \right\} \tag{8}$$

$$\mathrm{S}_{\mathrm{h}}^{k} = \left\{ \mathbf{P}_{\mathrm{h}} \in \left[\mathrm{L}^2\left(B_{0h}\right)\right]^2 |_{\left[\mathbf{P}_{\mathrm{h}}|_{\Omega_0^e} \in \mathbb{P}^k\left(\Omega_0^e\right)^2 \quad \forall \Omega_0^e \in B_{0h}\right]} \right\} \tag{9}$$

where $\mathbb{P}^k\left(\Omega_0^e\right)$ is the space of polynomial functions of order up to k with support in Ω_0^e. It is clear from these definitions that the polynomial order of approximation is the same for all three unknown fields [7]. It should be carefully noted that these spaces differ from the conventional finite element spaces in that they allow for jump discontinuities at interelement boundaries of polynomial order k.

We seek to define a discrete approximation $I_h(\boldsymbol{\varphi}_h, \mathbf{F}_h, \mathbf{P}_h)$ of the energy functional (5) $I(\boldsymbol{\varphi}, \mathbf{F}, \mathbf{P})$ on B_{0h} in the finite-dimensional spaces given in equations (7)-(9). To this end, we consider the contribution I_h^e of a generic element Ω_0^e in the subdivision B_{0h} to the total energy:

$$I_h(\boldsymbol{\varphi}_h, \mathbf{F}_h, \mathbf{P}_h) = \sum_{e}^{E} I_h^e(\boldsymbol{\varphi}_h^e, \mathbf{F}_h^e, \mathbf{P}_h^e) \tag{10}$$

with:

$$\begin{aligned} I_h^e \quad : \quad & \mathrm{H}^1(\Omega_0^e) \times \left[\mathrm{H}^1(\Omega_0^e)\right]^2 \times \left[\mathrm{H}^1(\Omega_0^e)\right]^2 \to \mathbb{R} : \\ & I_h^e(\boldsymbol{\varphi}_h^e, \mathbf{F}_h^e, \mathbf{P}_h^e) = \int_{\Omega_0^e} \left[W(\mathbf{C}_{\mathbf{h}}^{\mathbf{e}}) + \mathbf{P}_h^e : (\boldsymbol{\nabla}_0 \boldsymbol{\varphi}_h^e - \mathbf{F}_h^e) - \rho_0 \mathbf{B}_0 \cdot \boldsymbol{\varphi}_h^e \right] dV_0 - \\ & \int_{\partial_D \Omega_0^e} (\boldsymbol{\varphi}_h^e - \bar{\boldsymbol{\varphi}}_h) \cdot \mathbf{P}_h^e \cdot \mathbf{N} dS_0 - \int_{\partial_N \Omega_0^e} \bar{\mathbf{T}} \cdot \boldsymbol{\varphi}_h^e dS_0 - \\ & \frac{1}{2} \int_{\partial_I \Omega_0^e} \left(\boldsymbol{\varphi}_h^e - \boldsymbol{\varphi}_h^{ext}\right) \cdot \mathbf{P}_h^e \cdot \mathbf{N} dS_0 \end{aligned} \tag{11}$$

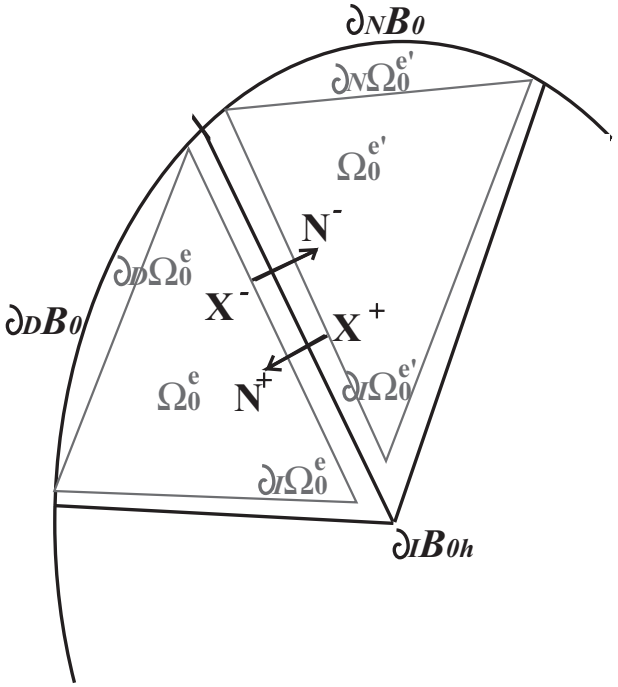

Figure 2. Details of two elements Ω_0^e and $\Omega_0^{e'}$ of the discretization B_{0h}. $\partial_D B_0$ is the Dirichlet boundary, $\partial_N B_0$ is the Neumann boundary, $\partial_I B_{0h}$ is the interior boundary of the discretization. The outward normals of the two elements are represented.

where the boundary of element Ω_0^e:

$$\begin{aligned}
&\partial\Omega_0^e = \partial_D\Omega_0^e \cup \partial_N\Omega_0^e \cup \partial_I\Omega_0^e \text{ with}\\
&\partial_D\Omega_0^e = \partial_D B_{0h} \cap \partial\Omega_0^e\\
&\partial_N\Omega_0^e = \partial_N B_{0h} \cap \partial\Omega_0^e, \text{ and}\\
&\partial_I\Omega_0^e = \partial_I B_{0h} \cap \partial\Omega_0^e,\\
&\partial_I B_{0h} = \left[\bigcup_{e=1}^{E} \partial\Omega_0^e\right]_{\setminus \partial B_{0h}}
\end{aligned} \tag{12}$$

The last term of equation (11) enforces weakly the interelement compatibility, where $\boldsymbol{\varphi}_h^{ext}$

represents the deformation of neighboring elements. The factor $\frac{1}{2}$ has been introduced in order to avoid duplication of the contribution of this term to the total energy. Here and subsequently, we will assume that the unknown fields can have jump discontinuities at interelement boundaries $\partial_I \Omega_0^e$. To this end, we introduce the jump $[\![\bullet]\!]$ and mean $\langle\bullet\rangle$ operators defined on the space of the trace of functions which can possibly adopt multiple values on the interior boundary $\mathrm{TR}(\partial_I B_{0h}) = \prod_{e=1}^{E} \left(\mathrm{L}^2\left(\partial_I \Omega_0^e\right)\right)$ [11]:

$$[\![\bullet]\!] \;:\; [\mathrm{TR}(\partial_I B_{0h})]^{1 \text{ or } 2} \rightarrow \left[\mathrm{L}^2\left(\partial_I B_{0h}\right)\right]^{1 \text{ or } 2}, \quad [\![\bullet]\!] = \bullet^+ - \bullet^- \tag{13}$$

$$\langle\bullet\rangle \;:\; [\mathrm{TR}(\partial_I B_{0h})]^{1 \text{ or } 2} \rightarrow \left[\mathrm{L}^2\left(\partial_I B_{0h}\right)\right]^{1 \text{ or } 2}, \quad \langle\bullet\rangle = \frac{1}{2}\left[\bullet^+ + \bullet^-\right] \tag{14}$$

In these expressions, the bullet represents a generic field,

$$\bullet^- = \lim_{\varepsilon \rightarrow 0_+} \bullet\left(\mathbf{X} - \varepsilon \mathbf{N}^-\right) \quad \forall \;\; \mathbf{X} \in \partial_I B_{0h} \tag{15}$$

$$\bullet^+ = \lim_{\varepsilon \rightarrow 0_+} \bullet\left(\mathbf{X} + \varepsilon \mathbf{N}^-\right) \quad \forall \;\; \mathbf{X} \in \partial_I B_{0h} \tag{16}$$

and $\mathbf{N}^-$ is conventionally defined as the reference outward unit normal of $\partial\Omega_0^e$, whereas $\mathbf{N}^+$ is the reference outward unit normal of its neighboring element $\Omega_0^{e'}$. Clearly, in (15) we have assumed $\mathbf{N}^- = -\mathbf{N}^+ \; \forall \; \mathbf{X} \in \partial_I B_{0h}$.

The discretized total energy functional given in equations (10) and (11) can then be rewritten as:

$$I_h \;:\; \mathrm{X}_\mathrm{h}^k \times \mathrm{S}_\mathrm{h}^k \times \mathrm{E}_\mathrm{h}^k \rightarrow \mathbb{R}$$

$$I_h(\boldsymbol{\varphi}_h, \mathbf{F}_h, \mathbf{P}_h) = \int_{B_{0h}} \left[W(\mathbf{C_h}) + \mathbf{P}_h : (\boldsymbol{\nabla}_0 \boldsymbol{\varphi}_h - \mathbf{F}_h) - \rho_0 \mathbf{B}_0 \cdot \boldsymbol{\varphi}_h\right] dV_0 - \int_{\partial_D B_{0h}} (\boldsymbol{\varphi}_h - \bar{\boldsymbol{\varphi}}_h) \cdot \mathbf{P}_h \cdot \mathbf{N} dS_0 - \int_{\partial_N B_{0h}} \bar{\mathbf{T}} \cdot \boldsymbol{\varphi}_h dS_0 + \int_{\partial_I B_{0h}} [\![\boldsymbol{\varphi}_h]\!] \cdot \langle \mathbf{P}_h \rangle \cdot \mathbf{N}^- dS_0 \tag{17}$$

since, providing $k \geq 1$, the interpolation spaces $\mathrm{X}_{\mathrm{h}}^{k}, \mathrm{S}_{\mathrm{h}}^{k}, \mathrm{E}_{\mathrm{h}}^{k}$ are subsets of $\mathrm{X}^{\mathrm{f}}\left(B_{0h}\right) = \prod_{e=1}^{E}\left(\mathrm{H}^{1}\left(\Omega_{0}^{e}\right)\right)$ and $\mathrm{S}^{\mathrm{f}}\left(B_{0h}\right) = \prod_{e=1}^{E}\left(\left[\mathrm{H}^{1}\left(\Omega_{0}^{e}\right)\right]^{2}\right)$, i.e. the spaces of all vectorial and tensorial functions belonging to H^{1} and $\left[\mathrm{H}^{1}\right]^{2}$ in each element, respectively.

The approximate solution to problem (1)-(4) is then found by finding the stationary points of the energy functional (17) with respect to variations $\delta\boldsymbol{\varphi}_h, \delta\mathbf{P}_h, \delta\mathbf{F}_h$ of the unknown fields in the constrained spaces:

$$\mathrm{X}_{\mathrm{hc}}^{k} = \left\{\delta\boldsymbol{\varphi}_h \in \mathrm{X}_{\mathrm{h}}^{k}|_{\left[\delta\boldsymbol{\varphi}_h|_{\partial_D B_{0h}}=0\right]}\right\} \tag{18}$$

$$\mathrm{S}_{\mathrm{hc}}^{k} = \left\{\delta\mathbf{P}_h \in \mathrm{S}_{\mathrm{h}}^{k}|_{\left[\delta\mathbf{P}_h|_{\partial_N B_{0h}}=0\right]}\right\} \tag{19}$$

$$\mathrm{E}_{\mathrm{hc}}^{k} = \left\{\delta\mathbf{F}_h \in \mathrm{E}_{\mathrm{h}}^{k}|_{\left[\delta\mathbf{F}|_{\partial_N B_{0h}}=0\right]}\right\} \tag{20}$$

leading respectively to the weak formulation of the equations of equilibrium, compatibility and constitutive behavior:

$$\begin{aligned} 0 = & \int_{B_{0h}} \mathbf{P}_h : \boldsymbol{\nabla}_0 \delta\boldsymbol{\varphi}_h dV_0 - \int_{B_{0h}} \rho_0 \mathbf{B}\cdot\delta\boldsymbol{\varphi}_h dV_0 - \\ & \int_{\partial_N B_{0h}} \bar{\mathbf{T}}\cdot\delta\boldsymbol{\varphi} dS_0 + \int_{\partial_I B_{0h}} [\![\delta\boldsymbol{\varphi}_h]\!]\cdot\langle\mathbf{P}_h\rangle\cdot\mathbf{N}^{-} dS_0 \quad \forall\delta\boldsymbol{\varphi}_h \in \mathrm{X}_{\mathrm{hc}}^{k} \end{aligned} \tag{21}$$

$$\begin{aligned} 0 = & \int_{B_{0h}} \delta\mathbf{P}_h : \left[\boldsymbol{\nabla}_0\boldsymbol{\varphi}_h - \mathbf{F}_h\right] dV_0 - \int_{\partial_D B_{0h}} \left[\boldsymbol{\varphi}_h - \bar{\boldsymbol{\varphi}}_h\right]\cdot\delta\mathbf{P}_h\cdot\mathbf{N} dS_0 + \\ & \int_{\partial_I B_{0h}} [\![\boldsymbol{\varphi}_h]\!]\cdot\langle\delta\mathbf{P}_h\rangle\cdot\mathbf{N}^{-} dS_0 \quad \forall\delta\mathbf{P}_h \in \mathrm{S}_{\mathrm{hc}}^{k} \end{aligned} \tag{22}$$

$$0 = \int_{B_{0h}} \left[2\mathbf{F}_h \frac{\partial W\left(\mathbf{C}_h\right)}{\partial\mathbf{C}} - \mathbf{P}_h\right] : \delta\mathbf{F}_h dV_0 \quad \forall\delta\mathbf{F}_h \in \mathrm{E}_{\mathrm{hc}}^{k} \tag{23}$$

where $2\frac{\partial W(\mathbf{C})}{\partial\mathbf{C}} = \mathbf{S}$ is the second Piola-Kirchhoff stress tensor. The constitutive law (23) may clearly be enforced strongly. After replacing its local form in equation (21) one obtains:

$$\begin{aligned} 0 = & \int_{B_{0h}} \mathbf{P}\left(\mathbf{F}_h\right) : \boldsymbol{\nabla}_0\delta\boldsymbol{\varphi}_h dV_0 - \int_{B_{0h}} \rho_0\mathbf{B}\cdot\delta\boldsymbol{\varphi}_h dV_0 - \\ & \int_{\partial_N B_{0h}} \bar{\mathbf{T}}\cdot\delta\boldsymbol{\varphi} dS_0 + \int_{\partial_I B_{0h}} [\![\delta\boldsymbol{\varphi}_h]\!]\cdot\langle\mathbf{P}\left(\mathbf{F}_h\right)\rangle\cdot\mathbf{N}^{-} dS_0 \quad \forall\delta\boldsymbol{\varphi}_h \in \mathrm{X}_{\mathrm{hc}}^{k} \end{aligned} \tag{24}$$

where $\mathbf{P}(\mathbf{F}_h) = \mathbf{F}_h \mathbf{S}(\mathbf{C}_h) = \mathbf{F}_h 2\frac{\partial W(\mathbf{C}_h)}{\partial \mathbf{C}}$ and represents the evaluation of the local form of the constitutive law at the discrete deformation gradient $\mathbf{F}_h$.

At this point, an assumed form of the deformation gradients is adopted extending to finite deformations of solids the assumed scalar gradients in Brezzi et al [9], see also [11]:

$$\mathbf{F}_h = \boldsymbol{\nabla}_0 \boldsymbol{\varphi}_h + \mathbf{R}_{\bar{\boldsymbol{\varphi}}_h}(\llbracket \boldsymbol{\varphi}_h \rrbracket) \tag{25}$$

where the tensorial operator $\mathbf{R}_{\bar{\boldsymbol{\varphi}}_h} : \mathrm{L}^2(\partial_I B_{0h}) \rightarrow \mathrm{S}^k_{\mathrm{h}}$ is defined as:

$$\int_{B_{0h}} \mathbf{R}_{\bar{\boldsymbol{\varphi}}_h}(\llbracket \mathbf{v} \rrbracket) : \boldsymbol{\tau} dV_0 = \int_{\partial_I B_{0h}} \llbracket \mathbf{v} \rrbracket \cdot \langle \boldsymbol{\tau} \rangle \cdot \mathbf{N}^- dS_0 + \int_{\partial_D B_{0h}} [\bar{\boldsymbol{\varphi}}_h - \mathbf{v}] \cdot \boldsymbol{\tau} \cdot \mathbf{N} dS_0 \quad \forall \boldsymbol{\tau} \in \mathrm{S}^k_{\mathrm{h}} \tag{26}$$

such that the compatibility equation (22) is satisfied automatically.

The resulting one-field discontinuous Galerkin approximation of the finite elasticity problem can be rewritten as finding $\boldsymbol{\varphi}_h \in \mathrm{X}^k_{\mathrm{h}}$ such that:

$$\begin{aligned} 0 &= \int_{B_{0h}} \mathbf{P}(\mathbf{F}_h) : \boldsymbol{\nabla}_0 \delta\boldsymbol{\varphi}_h dV_0 - \int_{B_{0h}} \rho_0 \mathbf{B} \cdot \delta\boldsymbol{\varphi}_h dV_0 - \\ &\quad \int_{\partial_N B_{0h}} \bar{\mathbf{T}} \cdot \delta\boldsymbol{\varphi}_h dS_0 + \int_{\partial_I B_{0h}} \llbracket \delta\boldsymbol{\varphi}_h \rrbracket \cdot \langle \mathbf{P}(\mathbf{F}_h) \rangle \cdot \mathbf{N}^- dS_0 \quad \forall \delta\boldsymbol{\varphi}_h \in \mathrm{X}^k_{\mathrm{hc}} \\ \mathbf{F}_h &= \boldsymbol{\nabla}_0 \boldsymbol{\varphi}_h + \mathbf{R}_{\bar{\boldsymbol{\varphi}}_h}(\llbracket \boldsymbol{\varphi}_h \rrbracket) \end{aligned} \tag{27}$$

2.1. Stabilization of the equations

There are at least two problems with the discrete formulation (27). The first problem is the appearance of spurious numerical instabilities introduced by the discontinuous formulation. A common solution to this problem is to introduce stabilizing terms in the energy functional. A second problem is the non-local character of the average stresses $\langle \mathbf{P}(\mathbf{F}_h) \rangle$. which results in extended stiffness matrix bandwidths and more complex implementations. Clearly, this problem is associated with the assumed form of the deformation gradients in terms of the

lifting operator $\mathbf{R}_{\bar{\boldsymbol{\varphi}}_h}$. A practicable solution to both problems may be found by redefining the assumed form of the deformation gradients in equation (25) in terms of the tensorial operator $\mathbf{r}_{\mathrm{s}\bar{\boldsymbol{\varphi}}_h} \ : \ \mathrm{L}^2\left(\partial_I B_{0h}\right) \rightarrow \mathrm{S}_{\mathrm{h}}^k$

$$\int_{B_{0h}} \mathbf{r}_{\mathrm{s}\bar{\boldsymbol{\varphi}}_h}\left(\llbracket \mathbf{v} \rrbracket\right) : \boldsymbol{\tau} dV_0 = \begin{cases} \int_{\mathrm{s}} \llbracket \mathbf{v} \rrbracket \cdot \langle \boldsymbol{\tau} \rangle \cdot \mathbf{N}^- dS_0 & \forall \boldsymbol{\tau} \in \mathrm{S}_{\mathrm{h}}^k \text{ and } \forall \mathrm{s} \in \partial_I B_{0h} \\ \int_{\mathrm{s}} \left[\bar{\boldsymbol{\varphi}}_h \cdot \boldsymbol{\tau} \cdot \mathbf{N} - \mathbf{v} \cdot \boldsymbol{\tau} \cdot \mathbf{N}\right] dS_0 & \forall \boldsymbol{\tau} \in \mathrm{S}_{\mathrm{h}}^k \text{ and } \forall \mathrm{s} \in \partial_D B_{0h} \\ 0 & \forall \boldsymbol{\tau} \in \mathrm{S}_{\mathrm{h}}^k \text{ and } \forall \mathrm{s} \in \partial_N B_{0h} \end{cases} \tag{28}$$

where "s" is an arbitrary element side. The deformation gradients may then be redefined as:

$$\mathbf{F}_h = \boldsymbol{\nabla}_0 \boldsymbol{\varphi}_h + \sum_{\mathrm{s}}^{N_{\mathrm{s}}} \mathbf{r}_{\mathrm{s}\bar{\boldsymbol{\varphi}}_h}\left(\llbracket \boldsymbol{\varphi}_h \rrbracket\right) \quad \text{and} \quad \mathbf{C}_h = \mathbf{F}_h^T \mathbf{F}_h \quad \text{in} \quad \Omega_0^e \tag{29}$$

$$\mathbf{F}_{\mathrm{s}} = \boldsymbol{\nabla}_0 \boldsymbol{\varphi}_h + \beta \mathbf{r}_{\mathrm{s}\bar{\boldsymbol{\varphi}}_h}\left(\llbracket \boldsymbol{\varphi}_h \rrbracket\right) \quad \text{and} \quad \mathbf{C}_{\mathrm{s}} = \mathbf{F}_{\mathrm{s}}^T \mathbf{F}_{\mathrm{s}} \quad \text{on } \mathrm{s} \in \partial\Omega_0^e \tag{30}$$

where N_{s} is the number of element sides.

Thus, the deformation gradients inside the elements and on the element interfaces are evaluated using expressions (29) and (30), respectively. As a result, inter-element quantities depend only on values in adjacent elements, thus increasing the sparsity of the stiffness matrix and simplifying the implementation. As shown below, the parameter β may be chosen such that the formulation is stable. The resulting stabilized problem can then be rewritten as finding $\boldsymbol{\varphi}_h \in \mathrm{X}_{\mathrm{h}}^k$:

$$\begin{aligned} 0 \ = \ & \int_{B_{0h}} \mathbf{P}\left(\mathbf{F}_h\right) : \boldsymbol{\nabla}_0 \delta\boldsymbol{\varphi}_h dV_0 - \int_{B_{0h}} \rho_0 \mathbf{B} \cdot \delta\boldsymbol{\varphi}_h dV_0 - \int_{\partial_N B_{0h}} \bar{\mathbf{T}} \cdot \delta\boldsymbol{\varphi}_h dS_0 + \\ & \sum_{\mathrm{s}} \int_{\mathrm{s} \in \partial_I B_{0h}} \llbracket \delta\boldsymbol{\varphi}_h \rrbracket \cdot \langle \mathbf{P}\left(\mathbf{F}_s\right) \rangle \cdot \mathbf{N}^- dS_0 \ \ \forall \delta\boldsymbol{\varphi}_h \in \mathrm{X}_{\mathrm{hc}}^k \end{aligned} \tag{31}$$

Here and subsequently it will be assumed without loss of generality that Dirichlet boundary conditions are enforced strongly as in conventional finite element approaches, i.e.:

$$\boldsymbol{\varphi}_h = \bar{\boldsymbol{\varphi}} \ \ \forall \mathbf{X} \in \partial_D B_{0h} \quad \text{which implies} \quad \mathbf{r}_{\mathrm{s}\bar{\boldsymbol{\varphi}}_h} = 0 \ \ \forall \mathrm{s} \in \partial_D B_{0h} \tag{32}$$

as the main interest is in the treatment of interelement discontinuities.

2.2. Elimination of the operators

At this point we frame the formulation above in a way that it can be integrated in a conventional finite element framework. To this end, we assume that the displacement jumps at element interfaces are small compared to the deformation and linearize the evaluations of the constitutive rules $\mathbf{P}(\mathbf{F}_h)$ and $\mathbf{P}(\mathbf{F}_s)$ at the discrete deformation gradients $\mathbf{F}_h$ and $\mathbf{F}_s$ with respect to the operators $\mathbf{r}_{\mathrm{s}\bar{\boldsymbol{\varphi}}}$:

$$\mathbf{P}(\mathbf{F}_h) \simeq \mathbf{P}(\boldsymbol{\nabla}_0\boldsymbol{\varphi}_h) + \mathbb{C}(\boldsymbol{\nabla}_0\boldsymbol{\varphi}_h) : (\mathbf{F}_h - \boldsymbol{\nabla}_0\boldsymbol{\varphi}_h) \tag{33}$$

where $\mathbb{C} = \frac{\partial \mathbf{P}}{\partial \mathbf{F}}$ are the Lagrangian tangent moduli and similarly for $\mathbf{P}(\mathbf{F}_s)$. It bears emphasis that this step does not affect the nonlinear character of the constitutive law or the consistency of the scheme, as, in the absence of jumps, the operators vanish and the exact equations are verified identically. Replacing (33) and denoting $\bar{\mathbf{F}}_h = \boldsymbol{\nabla}_0\boldsymbol{\varphi}_h$ and all tensorial quantities evaluated at $\bar{\mathbf{F}}_h$ with the convention $\bar{\bullet} = \bullet\left(\bar{\mathbf{F}}_h\right)$ the first term in equation (31) can be rewritten as:

$$\begin{aligned}\int_{B_{0h}} \mathbf{P}(\mathbf{F}_h) : \boldsymbol{\nabla}_0\delta\boldsymbol{\varphi}_h dV_0 &= \int_{B_{0h}} \Big[\bar{\mathbf{P}} : \boldsymbol{\nabla}_0\delta\boldsymbol{\varphi}_h + \sum_{\mathrm{s}} \mathbf{r}_{\mathrm{s}\bar{\boldsymbol{\varphi}}}([\![\boldsymbol{\varphi}_h]\!]) : \bar{\mathbb{C}} : \boldsymbol{\nabla}_0\delta\boldsymbol{\varphi}_h\Big] dV_0 \\ &= \int_{B_{0h}} \bar{\mathbf{P}} : \boldsymbol{\nabla}_0\delta\boldsymbol{\varphi}_h dV_0 + \int_{\partial_I B_{0h}} [\![\boldsymbol{\varphi}_h]\!] \cdot \langle \bar{\mathbb{C}} : \boldsymbol{\nabla}_0\delta\boldsymbol{\varphi}_h \rangle \cdot \mathbf{N}^- dS_0\end{aligned} \tag{34}$$

owing to the definition of $\mathbf{r}_{\mathrm{s}\bar{\boldsymbol{\varphi}}}$ in (28). Similarly, the last term in equation (31) can be rewritten as:

$$\sum_{\mathrm{s}} \int_{\mathrm{s}\in\partial_I B_{0h}} [\![\delta\boldsymbol{\varphi}_h]\!] \cdot \langle \mathbf{P}(\mathbf{F}_s)\rangle \cdot \mathbf{N}^- dS_0 = \int_{\partial_I B_{0h}} [\![\delta\boldsymbol{\varphi}_h]\!] \cdot \left\langle \bar{\mathbf{P}} \right\rangle \cdot \mathbf{N}^- dS_0 + \sum_{\mathrm{s}} \int_{\mathrm{s}\in\partial_I B_{0h}} [\![\delta\boldsymbol{\varphi}_h]\!] \cdot \left\langle \beta\bar{\mathbb{C}} : \mathbf{r}_{\mathrm{s}\bar{\boldsymbol{\varphi}}_h}([\![\boldsymbol{\varphi}_h]\!])\right\rangle \cdot \mathbf{N}^- dS_0 \tag{35}$$

By virtue of (28), the last term in (35) can be rewritten as:

$$\begin{aligned}\sum_{\mathrm{s}} \int_{\mathrm{s}\in\partial_I B_{0h}} [\![\delta\boldsymbol{\varphi}_h]\!] \cdot \left\langle \beta\bar{\mathbb{C}} : \mathbf{r}_{\mathrm{s}\bar{\boldsymbol{\varphi}}_h}([\![\boldsymbol{\varphi}_h]\!])\right\rangle \cdot \mathbf{N}^- dS_0 &= \sum_{\mathrm{s}} \int_{B_{0h}} \mathbf{r}_{\mathrm{s}\bar{\boldsymbol{\varphi}}_h}([\![\delta\boldsymbol{\varphi}_h]\!]) : \beta\bar{\mathbb{C}} : \mathbf{r}_{\mathrm{s}\bar{\boldsymbol{\varphi}}_h}([\![\boldsymbol{\varphi}_h]\!])\, dV_0 \\ &= \sum_{\mathrm{s}} \int_{\mathrm{s}\in\partial_I B_{0h}} [\![\boldsymbol{\varphi}_h]\!] \cdot \left\langle \beta\bar{\mathbb{C}} : \mathbf{r}_{\mathrm{s}\bar{\boldsymbol{\varphi}}_h}([\![\delta\boldsymbol{\varphi}_h]\!])\right\rangle \cdot \mathbf{N}^- dS_0 \end{aligned} \tag{36}$$

which exposes the symmetry of the stabilization term with respect to $[\![\boldsymbol{\varphi}_h]\!]$ and $[\![\delta\boldsymbol{\varphi}_h]\!]$. Recalling that $\mathbf{r}_{\mathrm{s}\bar{\boldsymbol{\varphi}}_h}$ is dimensionless, on the boundary we can assume that[†]:

$$\left\langle \beta\bar{\mathbb{C}} : \mathbf{r}_{\mathrm{s}\bar{\boldsymbol{\varphi}}_h}([\![\boldsymbol{\varphi}_h]\!])\right\rangle = \left\langle \beta\bar{\mathbb{C}}\right\rangle \cdot \mathbf{N}^- \cdot \frac{[\![\boldsymbol{\varphi}_h]\!]}{h_{\mathrm{s}}} \quad \forall \mathbf{X} \in \partial_I B_{0h} \tag{37}$$

where h_{s} is a characteristic length of the mesh:

$$h_{\mathrm{s}} = \min\left(\frac{|\Omega_0^{e-}|}{|\partial\Omega_0^{e-}|}, \frac{|\Omega_0^{e+}|}{|\partial\Omega_0^{e+}|}\right) \tag{38}$$

Using (37), the operator $\mathbf{r}_{\mathrm{s}\bar{\boldsymbol{\varphi}}_h}$ can be effectively eliminated from (35), leading to the following

[†]This relation is defined up to a multiplicative constant. But this constant is subsumed in β which will be determined by stability considerations.

simplified form:

$$\sum_{\mathrm{s}} \int_{\mathrm{s}\in\partial_I B_{0h}} [\![\delta\boldsymbol{\varphi}_h]\!] \cdot \langle \mathbf{P}\left(\mathbf{F}_s\right)\rangle \cdot \mathbf{N}^- dS_0 = \int_{\partial_I B_{0h}} [\![\delta\boldsymbol{\varphi}_h]\!] \cdot \left\langle \bar{\mathbf{P}} \right\rangle \cdot \mathbf{N}^- dS_0 + \sum_{\mathrm{s}} \int_{\mathrm{s}\in\partial_I B_{0h}} [\![\delta\boldsymbol{\varphi}_h]\!] \otimes \mathbf{N}^- \cdot \left\langle \frac{\beta}{h_{\mathrm{s}}} \bar{\mathbb{C}} \right\rangle \cdot [\![\boldsymbol{\varphi}_h]\!] \otimes \mathbf{N}^- dS_0 \quad (39)$$

The stabilized weak formulation is obtained from (31), (34) and (39) as:

$$\begin{aligned} 0 = &\int_{B_{0h}} \bar{\mathbf{P}} : \boldsymbol{\nabla}_0 \delta\boldsymbol{\varphi}_h dV_0 + \int_{\partial_I B_{0h}} [\![\boldsymbol{\varphi}_h]\!] \cdot \langle \bar{\mathbb{C}} : \boldsymbol{\nabla}_0 \delta\boldsymbol{\varphi}_h \rangle \cdot \mathbf{N}^- dS_0 \\ &- \int_{B_{0h}} \rho_0 \mathbf{B} \cdot \delta\boldsymbol{\varphi}_h dV_0 - \int_{\partial_N B_{0h}} \bar{\mathbf{T}} \cdot \delta\boldsymbol{\varphi}_h dS_0 \\ &+ \int_{\partial_I B_{0h}} [\![\delta\boldsymbol{\varphi}_h]\!] \cdot \left\langle \bar{\mathbf{P}} \right\rangle \cdot \mathbf{N}^- dS_0 + \sum_{\mathrm{s}} \int_{\mathrm{s}\in\partial_I B_{0h}} [\![\delta\boldsymbol{\varphi}_h]\!] \otimes \mathbf{N}^- \cdot \left\langle \frac{\beta}{h_{\mathrm{s}}} \bar{\mathbb{C}} \right\rangle \cdot [\![\boldsymbol{\varphi}_h]\!] \otimes \mathbf{N}^- dS_0 \end{aligned}$$

$$\forall \delta\boldsymbol{\varphi}_h \in \mathrm{X}^k_{\mathrm{hc}} \quad (40)$$

In this expression:

$$\mathbf{f}^{int} \cdot \delta\mathbf{x} = \int_{B_{0h}} \bar{\mathbf{P}} : \boldsymbol{\nabla}_0 \delta\boldsymbol{\varphi}_h dV_0 \quad (41)$$

$$\mathbf{f}^{ext} \cdot \delta\mathbf{x} = \int_{B_{0h}} \rho_0 \mathbf{B} \cdot \delta\boldsymbol{\varphi}_h dV_0 + \int_{\partial_N B_{0h}} \bar{\mathbf{T}} \cdot \delta\boldsymbol{\varphi}_h dS_0 \quad (42)$$

constitute respectively the conventional internal and external virtual work leading to the customary unmodified finite element arrays $\mathbf{f}^{int}$ and $\mathbf{f}^{ext}$, whereas the interelement boundary terms:

$$\mathbf{f}^I \cdot \delta\mathbf{x} = \int_{\partial_I B_{0h}} [\![\boldsymbol{\varphi}_h]\!] \cdot \langle \bar{\mathbb{C}} : \boldsymbol{\nabla}_0 \delta\boldsymbol{\varphi}_h \rangle \cdot \mathbf{N}^- dS_0 + \int_{\partial_I B_{0h}} [\![\delta\boldsymbol{\varphi}_h]\!] \cdot \left\langle \bar{\mathbf{P}} \right\rangle \cdot \mathbf{N}^- dS_0 + \sum_{\mathrm{s}} \int_{\mathrm{s}\in\partial_I B_{0h}} [\![\delta\boldsymbol{\varphi}_h]\!] \otimes \mathbf{N}^- \cdot \left\langle \frac{\beta}{h_{\mathrm{s}}} \bar{\mathbb{C}} \right\rangle \cdot [\![\boldsymbol{\varphi}_h]\!] \otimes \mathbf{N}^- dS_0 \quad (43)$$

denote the contributions of the discontinuous terms to the weak formulation, leading to the definition of the nodal array $\mathbf{f}^I$ contributing to the internal force array. In these expressions, $\mathbf{x}$ represents the array of deformed nodal coordinates and $\delta\mathbf{x}$ its corresponding variations.

As pointed out previously [10, 27], the first term in (43) only plays the role of symmetrizing the problem, see equation (36), and is not necessary, as the weak enforcement of the C^0 continuity at element interfaces is already taken care of by the quadratic stabilization term. This symmetrizing term may be taken as the starting point for the formulation of a rich variety of numerical fluxes resulting in improved rates of convergence in the L^2 norm—albeit not in the H space, see Appendix I.5 for linear problems [27]—. A comprehensive study on the choice of the numerical flux and of the symmetrization would be of interest but is beyond the purpose of the present work. On this premise and for simplicity and efficiency of the implementation, this term will be ignored hereinafter. It will be shown below, that the consistency and stability of the algorithm proposed is not affected by the absence of this term.

We conclude that the discontinuous Galerkin formulation for finite deformation of solids derived above results in the following form of numerical fluxes and stabilization terms at element interfaces:

$$\begin{aligned}\mathbf{f}^I \cdot \delta\mathbf{x} = &\int_{\partial_I B_{0h}} [\![\delta\boldsymbol{\varphi}_h]\!] \cdot \langle \bar{\mathbf{P}} \rangle \cdot \mathbf{N}^- dS_0 \\ &+ \sum_{\mathrm{s}} \int_{\mathrm{s}\in\partial_I B_{0h}} [\![\delta\boldsymbol{\varphi}_h]\!] \otimes \mathbf{N}^- \cdot \left\langle \frac{\beta}{h_{\mathrm{s}}} \bar{\mathbb{C}} \right\rangle \cdot [\![\boldsymbol{\varphi}_h]\!] \otimes \mathbf{N}^- dS_0\end{aligned} \tag{44}$$

The average numerical flux is of the form proposed by Bassi and Rebay [7] for fluids and the stabilization term is of the quadratic type and is based on a linearization of the constitutive law with respect to the displacement jumps. The first term ensures the consistency of the numerical scheme, whereas the second term enforces weakly interelement compatibility.

The resulting formulation corresponds exactly to an interior penalty method, including inter-element boundary integrals and additional terms arising from the discontinuous space of elements. In this regard, the derivation based on the lifting operator is not necessary but provides a rigorous and elegant means of deriving the equations from the general variational

principle for large deformations.

An analysis of the numerical properties of this formulation including consistency, stability and convergence rate is provided in Appendix I. Main result is that the method is stable provided β is larger than a constant depending only on the degree of the test functions.

3. FINITE ELEMENT IMPLEMENTATION

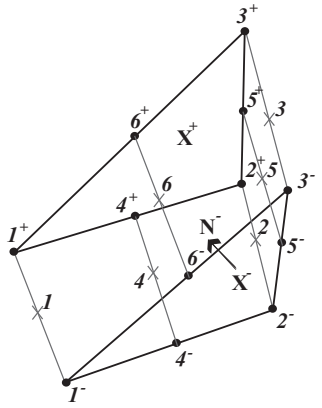

Figure 3. Interface element.

In this section, we take expression (44) as a basis for the formulation of interface elements providing a convenient means for implementation of the discontinuous Galerkin method proposed within a conventional finite element framework. It bears emphasis that in the formulation proposed the conventional finite elements inside the volume of the domain can be used without modification. For definiteness and ease of mesh generation, we adopt 10-node quadratic tetrahedral elements, i.e. the polynomial order of interpolations is $k = 2$.

These interface elements bear some resemblance in their geometric description to the so-

called cohesive elements proposed for problems involving fracture, [28]. At each and every interelement boundary an interface element is inserted by splitting the shared nodes which subsequently leads to independent problem unknowns. This new element encompasses the surface elements $\partial_I\Omega_0^{e+}$ and $\partial_I\Omega_0^{e-}$, determined by the surface nodes of the adjacent volumetric elements Ω_0^{e+} and Ω_0^{e-}, respectively, Figure 3. These two surface elements coincide in the reference configuration. In the particular case of ten-node tetrahedra, each surface element has $n = 6$ nodes and the resulting interface element $2n = 12$ nodes. However, the element formulation is extensible to arbitrary three-dimensional finite element interpolations.

In the reference configuration, the interpolation of the position, the deformation mapping and its jumps is done using the standard shape functions of the surface element $N_a(\boldsymbol{\xi}), a \in [1, n]$, where $\boldsymbol{\xi} = (\xi_1, \xi_2)$ are the natural coordinates. Thus,

$$\mathbf{X}^{\pm}(\boldsymbol{\xi}) = \sum_{a=1}^{n} N_a(\boldsymbol{\xi})\mathbf{X}_a^{\pm} \tag{45}$$

$$[\![\boldsymbol{\varphi}_h]\!](\boldsymbol{\xi}) = \sum_{a=1}^{n} N_a(\boldsymbol{\xi})\left[\mathbf{x}_a^{+} - \mathbf{x}_a^{-}\right] \tag{46}$$

$$[\![\delta\boldsymbol{\varphi}_h]\!](\boldsymbol{\xi}) = \sum_{a=1}^{n} N_a(\boldsymbol{\xi})\left[\delta\mathbf{x}_a^{+} - \delta\mathbf{x}_a^{-}\right] \tag{47}$$

where $\mathbf{X}_a^{\pm}$ and $\mathbf{x}_a^{\pm}, a \in [1, n]$ are the nodal coordinates of the surface elements in the reference and deformed configuration, respectively. The interelement outer surface normal $\mathbf{N}^-$ corresponding to element Ω_0^{e-} evaluated on the middle surface is obtained from the following expression:

$$\mathbf{N}^{-}(\boldsymbol{\xi}) = \frac{\mathbf{G}_1(\boldsymbol{\xi}) \times \mathbf{G}_2(\boldsymbol{\xi})}{|\mathbf{G}_1(\boldsymbol{\xi}) \times \mathbf{G}_2(\boldsymbol{\xi})|} \tag{48}$$

in which

$$\mathbf{G}_\alpha(\boldsymbol{\xi}) = \mathbf{X}_{,\alpha} = \sum_{a=1}^{n} N_{a,\alpha}(\boldsymbol{\xi})\mathbf{X}_a \tag{49}$$

are the tangent basis vectors, $\alpha \in [1,2]$, $\mathbf{X}_a = \frac{\mathbf{X}_a^+ + \mathbf{X}_a^-}{2}$ and similarly $\mathbf{x}_a = \frac{\mathbf{x}_a^+ + \mathbf{x}_a^-}{2}$. When interpolations (45)-(47) are inserted in (44), the following expression for the nodal force array follows:

$$\begin{aligned} \mathbf{f}_a^{I\pm} = &\pm \int_{\partial_I B_{0h}} \left\langle \bar{\mathbf{P}} \right\rangle \cdot \mathbf{N}^- N_a dS_0 \\ &\pm \int_{\partial_I B_{0h}} \left[\left\langle \frac{\beta}{h_{\mathrm{s}}} \bar{\mathbb{C}} \right\rangle : [\![\mathbf{x}_b]\!] \otimes \mathbf{N}^- \right] \cdot \mathbf{N}^- N_a N_b dS_0 \end{aligned} \tag{50}$$

where $[\![\mathbf{x}_a]\!] = \mathbf{x}_a^+ - \mathbf{x}_a^-$ are the jumps in the deformed nodal coordinates. The average Piola-Kirchhoff stresses and Lagrangian tangent moduli in (50) are computed after extrapolation from the quadrature points of the adjacent elements Ω_0^{e+} and Ω_0^{e-} to the element nodes. This requires the assembly and update of the conventional bulk elements first. Nodal values are used to compute averages and jumps appearing in expression (50) which, in turn, are interpolated onto the surface element integration points. The value of h_{s} is obtained from the two neighboring elements as required by equation (38).

The integral in (50) is evaluated using the 3-point Gauss quadrature rule. In static calculations, as is the focus of this work, a consistent linearization of this expression leading to the computation of the stiffness matrix enables a Newton-Raphson solution of the system of nonlinear algebraic equations in the deformed nodal coordinates:

$$\mathbf{f}^{int}(\mathbf{x}) + \mathbf{f}^{I}(\mathbf{x}) = \mathbf{f}^{ext} \tag{51}$$

resulting from (41), (50) and (42). The expression of the consistent tangent stiffness matrix is provided in Appendix II.

A particularly attractive aspect of the proposed implementation of the discontinuous Galerkin method in terms of interface elements is its compatibility with the conventional bulk finite elements framework.

Table I. Geometric and material properties of the beam problem

Properties	Values
Length	$L = 1m$
Height	$h = 0.1m$
Initial Young modulus	$E_0 = 200GPa$
Initial Poisson ratio	$\nu_0 = 0.3$

4. NUMERICAL EXAMPLES

In this section, we present three-dimensional numerical examples with the intent of demonstrating the feasibility of the DG framework for large deformations of solids and of providing numerical evidence of the established properties of the method.

The examples correspond to the static deformation of a three-dimensional cantilever elastic beam structure subjected to different loading conditions. The first example tests the accuracy and stability of the method in the infinitesimal linear limit. In the second example we study the convergence of the method for a non-linear problem involving large deformations. In the last example, we illustrate the robustness of the method in a problem involving very large deformations. In all cases, the simulation results of the discontinuous Galerkin method are compared with the corresponding continuous case. We recall that the purpose of this paper is to provide a starting point for simulating physical discontinuities in non-linear mechanics. The authors believe that discontinuous Galerkin method can be this framework. So we are just interested in showing that the method is robust and accurate. We do not want to show that the method is more efficient than other ones.

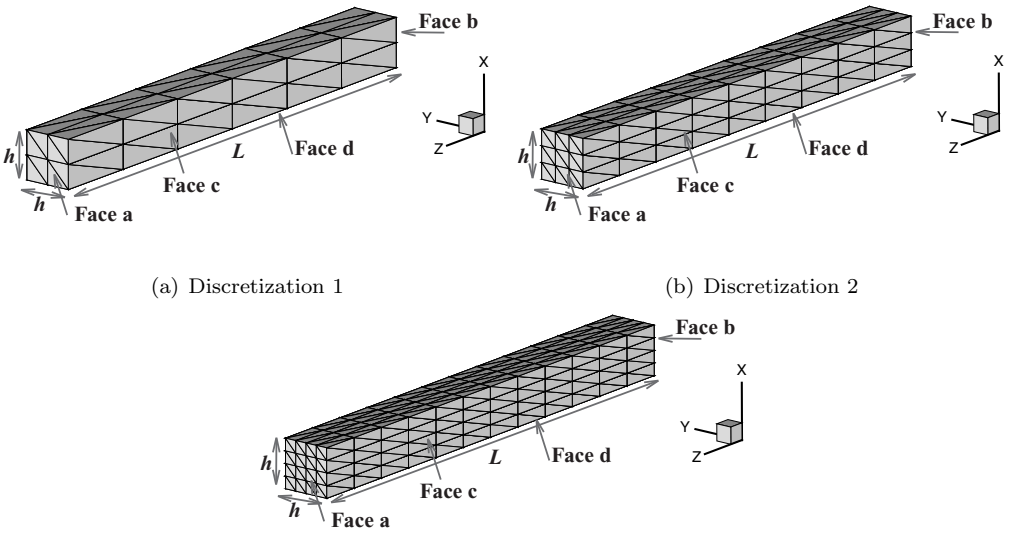

(a) Discretization 1

(b) Discretization 2

(c) Discretization 3

Figure 4. Beam problem description and discretizations employed.

In these calculations the material model corresponds to a Neohookean model extended to the compressible range. The strain energy density function is:

$$W = \left(\frac{\lambda}{2}\log J - \mu\right)\log J + \frac{\mu}{2}(I_1 - 3) \tag{52}$$

where λ and μ are the material parameters, $J = \det(\mathbf{F})$ and $I_1 = tr(\mathbf{C})$. The material parameters and the geometric characteristics of the beam used in calculations are listed in Table I.

The beam geometry and the three different finite element meshes employed are shown in Figure 4. The mesh statistics are reported in Table II both for the continuous and discontinuous Galerkin case.

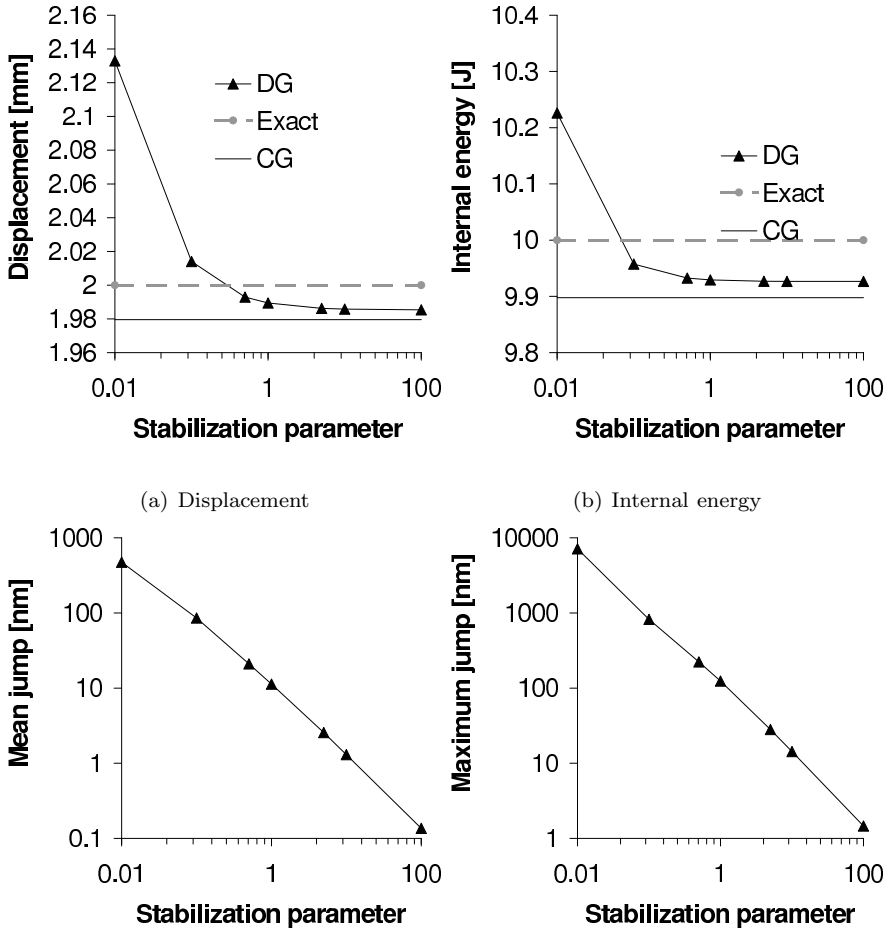

(a) Displacement

(b) Internal energy

(c) Mean interelement displacement jump

(d) Maximum interelement displacement jump

Figure 5. Comparison of simulation results against exact solution for a cantilever beam showing the influence of the stabilization parameter on the accuracy of the proposed method. The corresponding continuous simulation using the same discretization is shown for reference. In the legends, DG and CG stand for discontinuous and continuous Galerkin, respectively.

Table II. Beam problem discretization details.

Discretization	elements	nodes CG	nodes DG	ratio
1	144	325	1440	4.4
2	486	931	4860	5.2
3	1152	2025	11520	5.7

4.1. Small deflections of a cantilever beam with a tip load

In this first example the beam is clamped on face b as shown in Figure 4 and loaded with a distributed load $F = 10kN$ at the tip (face a). According to classic beam theory the tip deflection is $\delta = 4\frac{L^3}{h^4}\frac{F}{E_0} = 2mm$, the work of the external load is $W_{\text{ext}} = F\ \delta = 20J$ and the internal energy is $W_{\text{int}} = \frac{F\ \delta}{2} = 10J$.

A first simulation was done with the stabilization parameter $\beta = 0$ which confirmed that the method is unstable in this case. A series of simulations was conducted using the intermediate mesh size, Figure 4, for different values of the parameter $\beta \in [0.01, 100]$, confirming that the method is stable for β larger than a constant, as shown in Appendix I.4. Moreover, the numerical results suggest that this constant is small. A comparison of the exact values of the tip deflection and internal energy with the simulation results is given in Figures 5(a) and 5(b), respectively. It can be seen in these figures that for small values of β the predicted deflection is larger than the exact one, a direct consequence of the fact that the interelement compatibility is enforced weakly. As the β parameter is increased, the discontinuous Galerkin solution converges to the continuous simulation result for the adopted discretization, as expected. Figures 5(c)-(d) show that the average and maximum size of the displacement jumps decrease

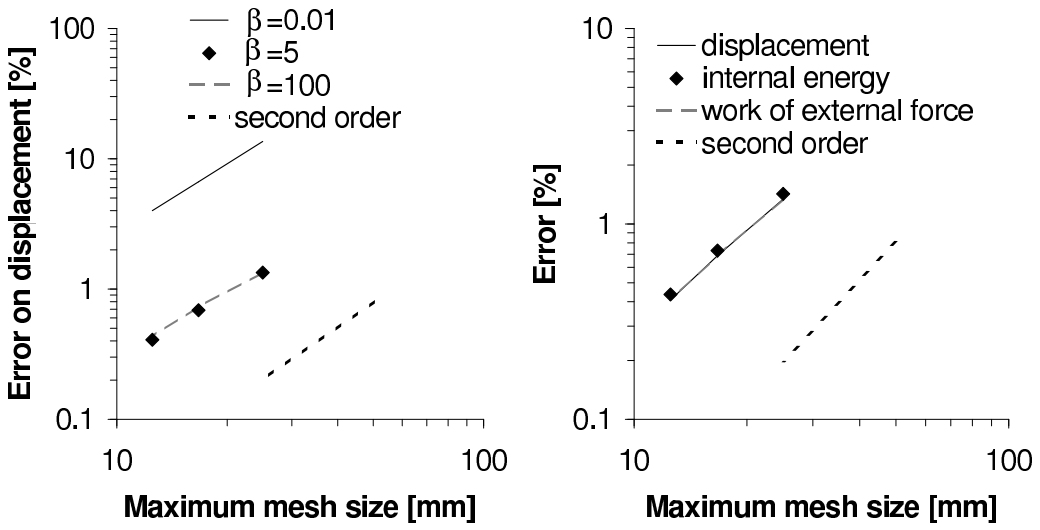

(a) error on tip deflection

(b) errors for $\beta = 5$

Figure 6. Convergence analysis of the discontinuous Galerkin method applied to the cantilever beam problem. The plot shows the error vs. mesh size h. The theoretical convergence rate ($O(h^k), k = 2$) is observed.

as β increases at a rate between $\frac{1}{2}$ and 1. It bears emphasis that even for very small values of the stabilization parameter the method remains stable while interelement displacement jumps stay small ($\sim 10^{-3}$ of the tip deflection at most).

An analysis of the convergence properties of the method is presented in Figure 6. This analysis consisted of conducting simulations with different mesh sizes as described in Table II. When analysing the tip deflection for different values of β (Figure 6a), it can be seen that for $\beta = 0.01$ the method is unstable and the displacement is overestimated (Figure 5a). For larger value of β the theoretical convergence rate is obtained, as expected. This is true for the tip displacement but also for the energy norms (Figure 6b). We can conclude that, as the theory is predicting it, the method is stable and converge only for β larger than a constant that depends

only on the polynomial degree. The value $\beta = 5$ leads to stability and convergence.

4.2. Large deflections of a cantilever beam

In this example the load applied to the beam is increased by a factor of 1000, i.e., $F = 10MN$. The purpose of this test is to assess the accuracy and stability of the method under non-linear—albeit physically-stable—conditions. The medium-size mesh (Mesh 2) is employed both in the continuous and discontinuous simulations and the load is applied in increments of $0.1MN$. Figure 7 shows the deformed configuration and contours of internal energy density for three different values of the stabilization parameter $\beta = 0.5, 5$ and 100 as well as the corresponding continuous simulation result. As it can be observed in these figures, these simulations yield stable results which are similar to the continuous numerical solution. Figure 8 shows the deformed configurations obtained with the three different discretizations in Table II and $\beta = 5$. Figure 8(d) shows a detail illustrating the discontinuities at interelement boundaries. A quantitative analysis of the influence of the discretization and the stabilization parameter on the simulation results is presented in Figures 9 and 10. Figures 9(a) and (b) compares respectively the values of the tip deflection and internal energy with the corresponding continuous simulation as the stabilization parameter β is increased from 0.5 to 100. It can be observed that the method is stable even in the presence of nonlinearities at least insofar as no physical instabilities due to the nonlinearity appear in the problem, as expected in continuous formulations. As in the linear case, small values of the stabilization parameter β yield stable results and the discontinuous solution approaches the continuous result as β increases.

Figures 10(a)-(b) show the convergence of the weak enforcement of compatibility at interelement boundaries with the stabilization β. Average and maximum interelement

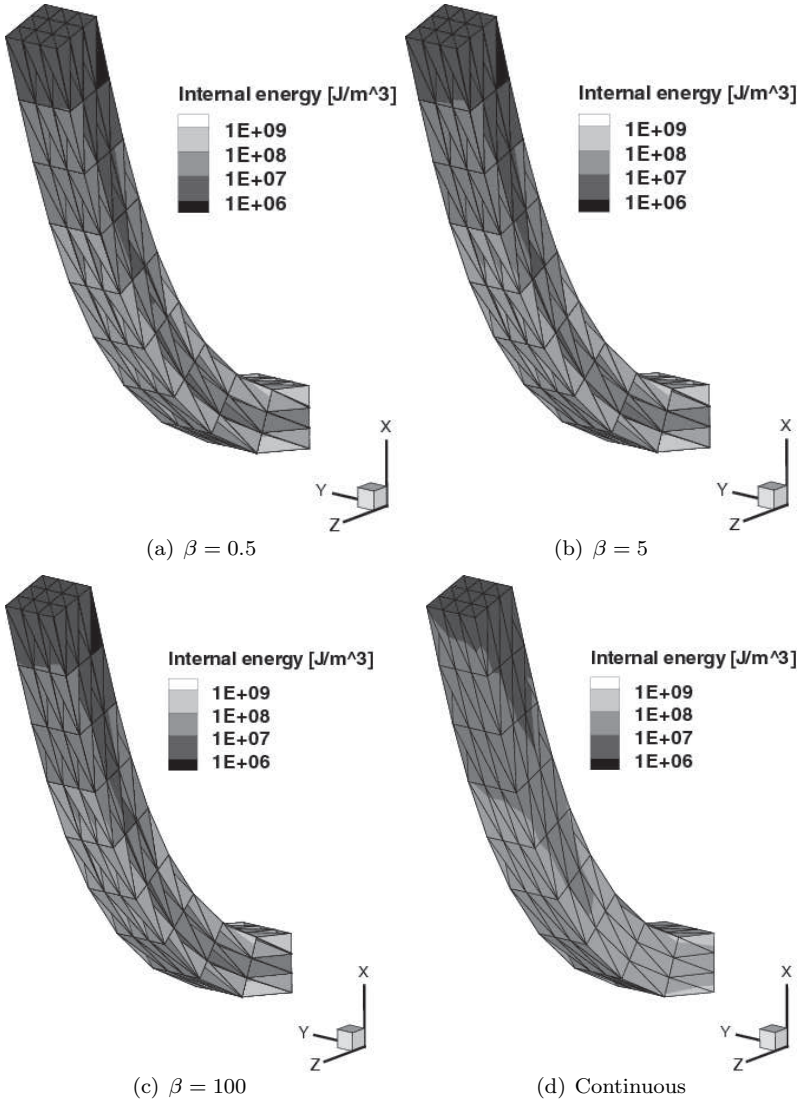

(a) $\beta = 0.5$ (b) $\beta = 5$

(c) $\beta = 100$ (d) Continuous

Figure 7. Deformed configuration and contours of internal energy density of cantilever beam subjected to a tip load $F = 10MN$. The figures show that the solution obtained with the discontinuous method with different values of the stabilization parameter is similar to the continuous solution.

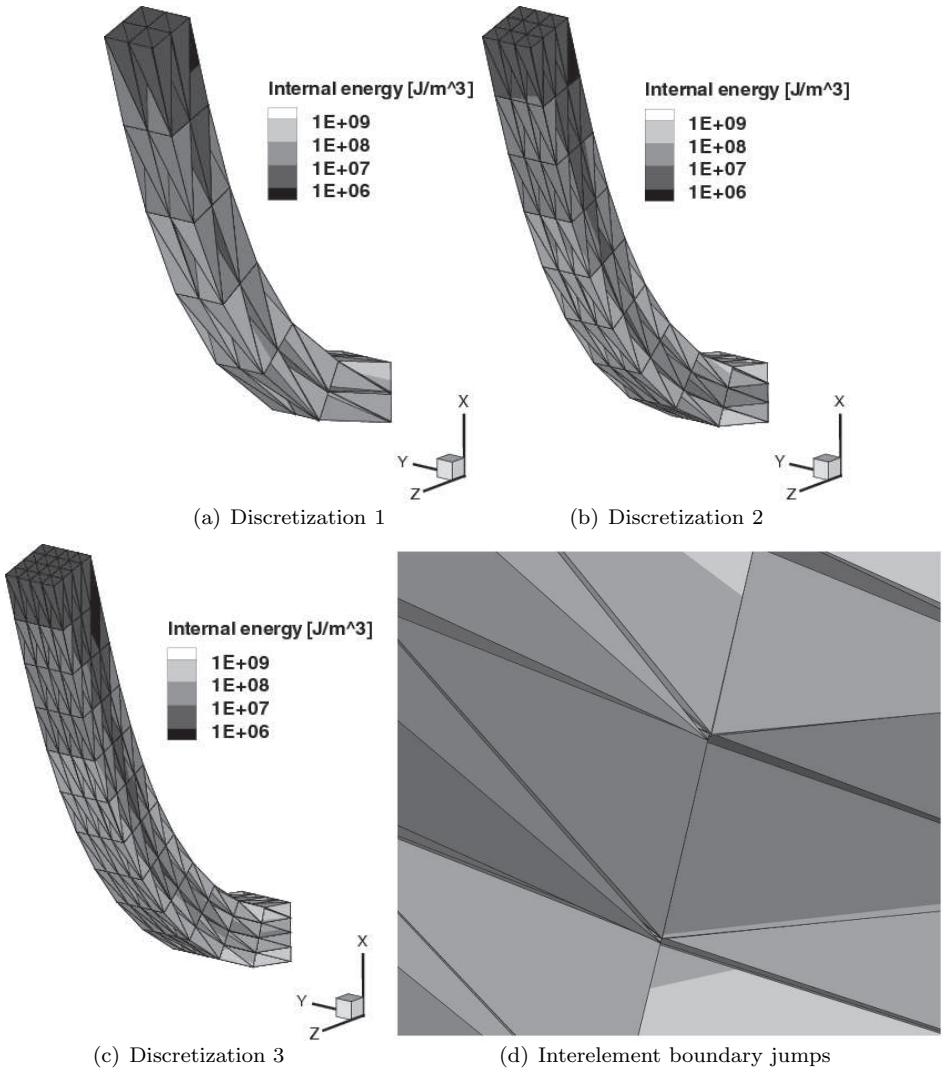

(a) Discretization 1 (b) Discretization 2

(c) Discretization 3 (d) Interelement boundary jumps

Figure 8. Deformed configuration and contours of internal energy density of cantilever beam subjected to a tip load $F = 10MN$ for different mesh sizes and $\beta = 5$ (a)-(c). Detail illustrating the discontinuities at interelement boundaries (d).

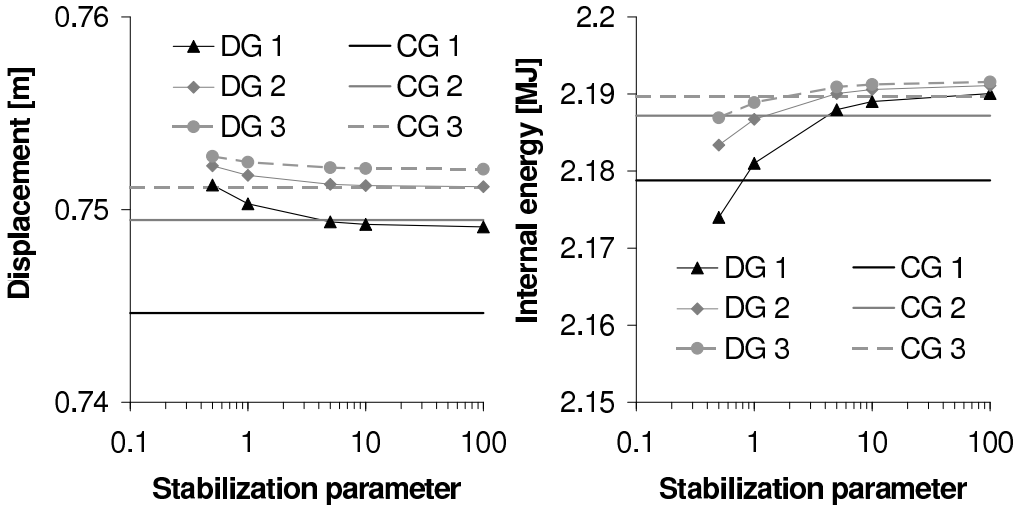

(a) Tip deflection

(b) Internal energy

Figure 9. Comparison of tip deflection and internal energy vs stabilization parameter against continuous simulation results in the case of large beam deflections. The different curves labeled DG1-3 and CG1-3 correspond to the different discretizations used in the discontinuous and continuous simulations, respectively.

displacement jumps decrease as β increases at a rate between $\frac{1}{2}$ and 1. Additional insight into the stability exhibited by the method can be gained by observing the number of Newton-Raphson iterations required to achieve convergence in the solution of the nonlinear algebraic equations (51), Figure 11. As this figure shows, the continuous method requires three iterations for all three mesh sizes. In the discontinuous case, one more iteration is necessary providing the interelement compatibility is enforced strictly through a large-enough value of the stabilization parameter β. This confirms that our approximation of the consistent stiffness matrix which only considers the geometric contribution, see Appendix II, does not affect the convergence within the stable range of β while it provides significant computational savings.

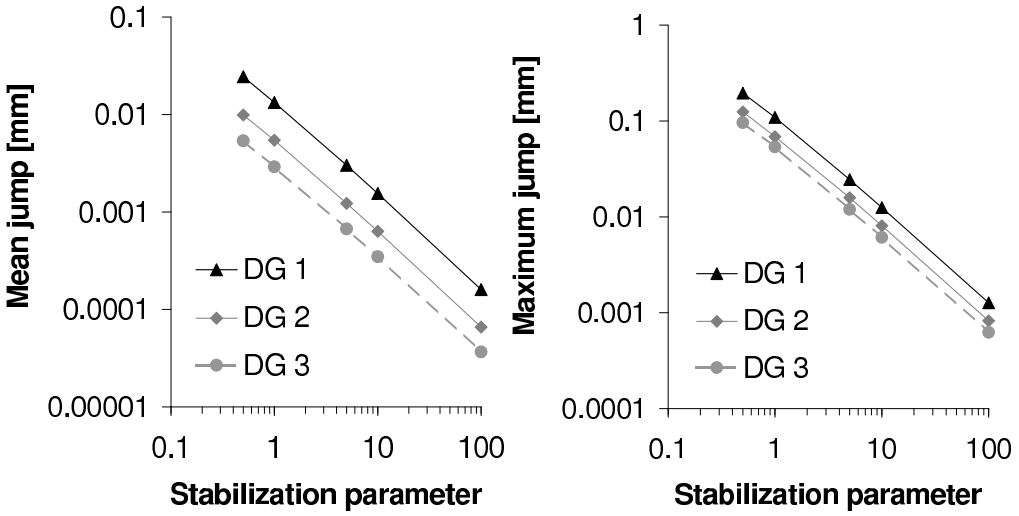

(a) Mean interelement displacement jump (b) Maximum interelement displacement jump

Figure 10. Influence of stabilization parameter on size of interelement jumps in the case of large beam deflections

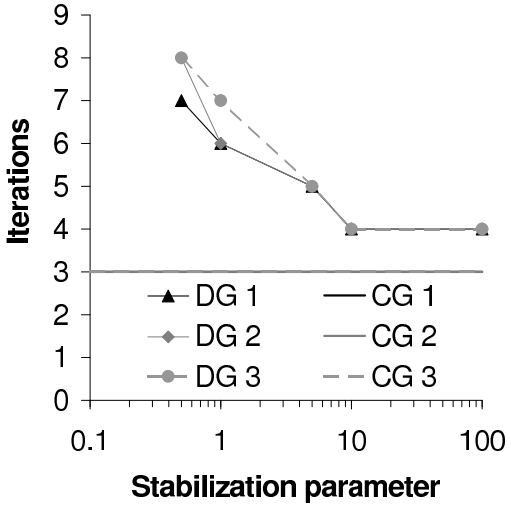

Figure 11. Number of Newton-Rapshon iterations to convergence vs stabilization parameter and comparison with iterations in continuous method.

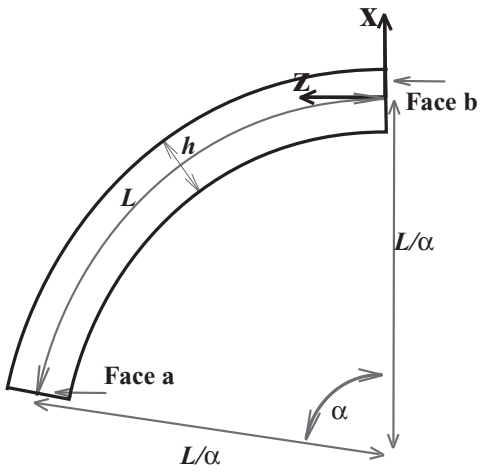

Figure 12. Description of the pure bending of the beam.

4.3. Large strains of a cantilever beam under pure bending

The third example is intended to illustrate the ability of the proposed method to describe very large deflections and strains, thus fully exhibiting its stability and accuracy properties under strong nonlinearity. The problem considered consists of imposing continuously-increasing pure bending Dirichlet boundary conditions at the end of a cantilever beam, see Figure 12. The deformation of the material surface $X_3 = L$ (face (a)) is imposed according to the restricted deformation mapping $\mathbf{x} = \boldsymbol{\varphi}(\mathbf{X}),\ X_3 = L$:

$$\begin{aligned} x_1(X_1;\alpha) &= X_1 + \left[\frac{L}{\alpha} + X_1\right][\cos(\alpha) - 1] \\ x_3(X_1;\alpha) &= \left[\frac{L}{\alpha} + X_1\right]\sin(\alpha) \end{aligned} \tag{53}$$

where α is the angle of rotation. The structure is free to move in direction x_2. The discretization employed is the second one. An angle $\alpha = 2\pi$ is reached in 500 load increments. The discontinuous Galerkin simulations are conducted with $\beta = 100$.

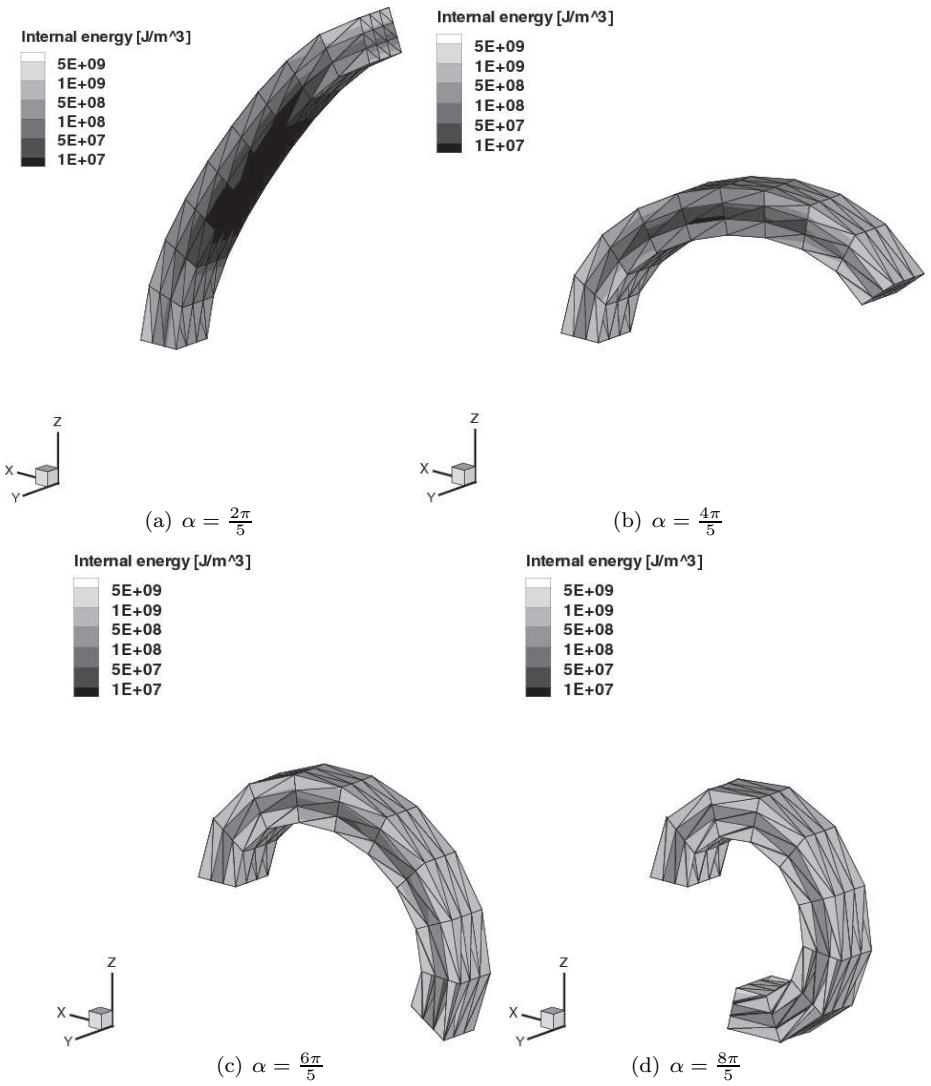

(a) $\alpha = \frac{2\pi}{5}$ (b) $\alpha = \frac{4\pi}{5}$

(c) $\alpha = \frac{6\pi}{5}$ (d) $\alpha = \frac{8\pi}{5}$

Figure 13. Snapshots of the deformed mesh configurations and contours of internal energy density at $\alpha = \frac{2\pi}{5}, \frac{4\pi}{5}, \frac{6\pi}{5}, \frac{8\pi}{5}$ during the simulation of the pure bending of a cantilever beam under large deformations using the discontinuous Galerkin method.

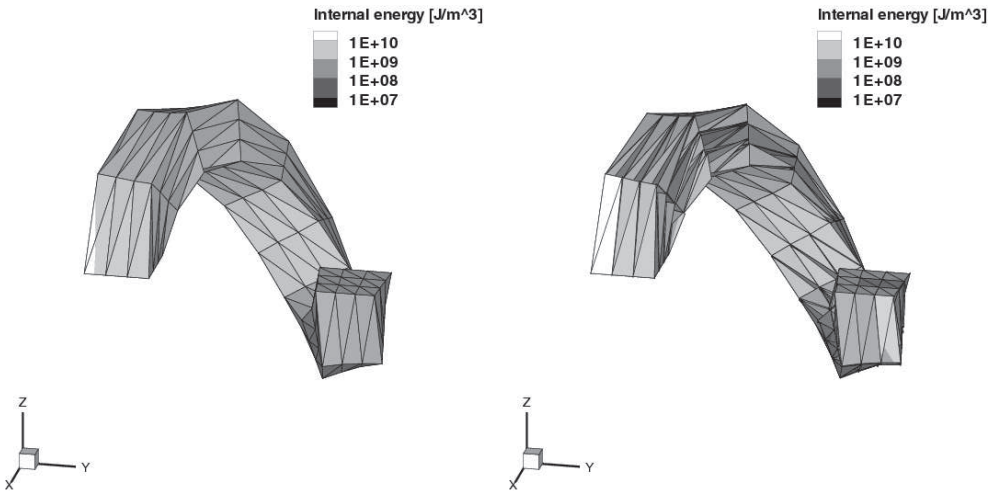

(a) Continuous Galerkin (b) Discontinuous Galerkin

Figure 14. Density of internal energy for pure bending of the beam: formation of a ring.

A series of snapshots of the deformed mesh configurations and spatial distribution of the internal energy density are shown in Figure 13. Figure 14 shows the final configuration after a total rotation of $\alpha = 2\pi$. Interestingly, both continuous and discontinuous simulations predict a helical shape with an out-of-plane deflection in the x_2 direction. The direction of the out-of-plane displacements chosen naturally by the computation is due to the asymmetry of the mesh. As it can be seen in the figure, both methods lead ostensibly to the same solution. A comparison of the total strain energy obtained with the continuous simulation ($31.8MJ$) vs. the discontinuous simulation ($31.3MJ$) yields a difference of only 1.5%, thus confirming the statement above. The mean and maximum interelement displacement jump obtained in this computation are very small, $0.48\mu m$ and $7.4\mu m$, respectively.

5. SUMMARY AND CONCLUSIONS

A formulation of the discontinous Galerkin method applied to large-deformation hyperelasticity has been presented. Key elements of the formulation include taking a three-field Hu-Washizu-de Veubeke energy functional allowing for jump discontinuities inside the problem domain as a starting point, the reduction to a single-field formulation involving formal jump operators and the linearization of the equations with respect to the jumps which effectively enables the elimination of the formal operators and leads to the possibility of practicable implementations.

The method thus formulated results in interelement boundary terms involving average-type fluxes and a stabilization term of the quadratic-type. The proposed method is shown to be consistent in the non-linear range. In the linear limit, this formulation can be reduced to a bilinear form as commonly found in discontinuous Galerkin methods. The L^2-stability and convergence properties of the method are demonstrated in this case. In the non-linear range these properties are expected. But when dealing with non-linear materials, these properties cannnot be generalized but are expected.

A three-dimensional implementation of the method in terms of interface elements located at interelement boundaries is described. A specially attractive aspect of this implementation is that it fits naturally within a conventional finite element framework. Examples of application to a beam structure and comparisons against the corresponding continuous numerical results in both the linear and large-deformation range are presented demonstrating the accuracy, stability and robustness of the method.

Since the discontinuous Galerkin method proposed is robust and can be easily implemented, we believe that it can be used as a starting point to simulate problems involving physical

discontinuity (failure, eg) in the non-linear range.

APPENDIX
I. NUMERICAL PROPERTIES

In this appendix the numerical properties of the proposed formulation are analyzed. The consistency of the method in the non-linear range is demonstrated. As is also common in conventional finite element methods for large deformations of solids, the analysis of stability is restricted to the linearized version of the numerical method. To this end, the linearized L^2-stability and convergence rate are also proven.

I.1. Consistency

From relations (41), (42) and (44), the weak formulation (31) is rewritten as finding $\boldsymbol{\varphi}_h \in \mathrm{X}_{\mathrm{h}}^k$ such that:

$$\begin{aligned}\int_{B_{0h}} \mathbf{P}\left(\bar{\mathbf{F}}\right) : \nabla_0 \delta\boldsymbol{\varphi}_h dV_0 + \\ \int_{\partial_I B_{0h}} [\![\delta\boldsymbol{\varphi}_h]\!] \otimes \mathbf{N}^- : \left\langle \frac{\beta}{h_{\mathrm{s}}} \bar{\mathbb{C}} \right\rangle : [\![\boldsymbol{\varphi}_h]\!] \otimes \mathbf{N}^- dS_0 + \int_{\partial_I B_{0h}} [\![\delta\boldsymbol{\varphi}_h]\!] \cdot \left\langle \mathbf{P}\left(\bar{\mathbf{F}}\right)\right\rangle \cdot \mathbf{N}^- dS_0 = \\ \int_{B_{0h}} \rho_0 \mathbf{B} \cdot \delta\boldsymbol{\varphi}_h dV_0 + \int_{\partial_N B_{0h}} \bar{\mathbf{T}} \cdot \delta\boldsymbol{\varphi}_h dS_0 \quad \forall \delta\boldsymbol{\varphi}_h \in \mathrm{X}_{\mathrm{h}c}^k \end{aligned} \tag{54}$$

If $\boldsymbol{\varphi}_h = \boldsymbol{\varphi}$ is the continuous exact solution, and if $\mathbf{P}\left(\nabla_0 \boldsymbol{\varphi}\right)$ is continuous, one has:

$$\begin{aligned} [\![\boldsymbol{\varphi}_h]\!] &= 0 \\ \bar{\mathbf{F}} &= \nabla_0 \boldsymbol{\varphi} \\ \left\langle \mathbf{P}\left(\bar{\mathbf{F}}\right)\right\rangle &= \mathbf{P}\left(\bar{\mathbf{F}}\right) \end{aligned} \tag{55}$$

Therefore using the divergence theorem, (18) and (54) leads to:

$$-\int_{B_{0h}} \nabla_0 \cdot \mathbf{P}\left(\bar{\mathbf{F}}\right) \cdot \delta\boldsymbol{\varphi}_h dV_0 + \int_{\partial_N B_{0h}} \delta\boldsymbol{\varphi}_h \cdot \mathbf{P}\left(\bar{\mathbf{F}}\right) \cdot \mathbf{N} dS_0 - \int_{\partial_I B_{0h}} [\![\delta\boldsymbol{\varphi}_h]\!] \cdot \mathbf{P}\left(\bar{\mathbf{F}}\right) \cdot \mathbf{N}^- dS_0 + \int_{\partial_I B_{0h}} [\![\delta\boldsymbol{\varphi}_h]\!] \cdot \mathbf{P}\left(\bar{\mathbf{F}}\right) \cdot \mathbf{N}^- dS_0 = \int_{B_{0h}} \rho_0 \mathbf{B} \cdot \delta\boldsymbol{\varphi}_h dV_0 + \int_{\partial_N B_{0h}} \bar{\mathbf{T}} \cdot \delta\boldsymbol{\varphi}_h dS_0 \quad \forall \delta\boldsymbol{\varphi}_h \in \mathrm{X}^k_{\mathrm{h}c} \tag{56}$$

It is clear that after elimination of the interelement boundary terms, the strong form of the equilibrium equations for large deformations of continua is recovered:

$$\nabla_0 \cdot \mathbf{P} + \rho_0 \mathbf{B} = 0 \quad \text{in } B_{0h} \tag{57}$$

$$\mathbf{P} \cdot \mathbf{N} = \bar{\mathbf{T}} \quad \text{on } \partial_N B_{0h} \tag{58}$$

Let us note that if the stress tensor is not continuous there is a lack in the consistency. However, in the linear range, by proceeding as Lew et al [11] (Corollary 3.12), and by using further results obtained in the linear range, one can show that the lack of consistency is bounded, that the stability is still verified, and that the convergence rate is still the same.

I.2. Reduction to linear elasticity

Let $\boldsymbol{\varepsilon}$ be the small strain tensor, and let us assume small displacements. The actual configuration is close to the reference configuration. Therefore the strain tensor is defined by:

$$\boldsymbol{\varepsilon}(\boldsymbol{\varphi}) = \frac{1}{2}\left[\nabla\boldsymbol{\varphi} + \boldsymbol{\varphi}\nabla\right] - \mathbf{I} \tag{59}$$

where $\mathbf{I}$ is the identity tensor. Let $\mathcal{H}$ be the classical Hooke tensor. When reducing to linear elasticity, one has:

$$\mathbb{C}_{iJkL} = \frac{\partial \mathbf{P}_{iJ}}{\partial \mathbf{F}_{kL}} = \mathbf{I}_{ik}\mathbf{P}_{JL} + 4\mathbf{F}_{iM}\frac{\partial^2 W}{\partial \mathbf{C}_{MJ}\partial \mathbf{C}_{NL}}\mathbf{F}_{kN} \simeq \mathcal{H} \tag{60}$$

since the geometrical term leads to a higher-order term. Then relation (54) is reduced to:

$$\begin{array}{c}\int_{B_h}\boldsymbol{\varepsilon}\left(\boldsymbol{\varphi}_h\right):\mathcal{H}:\nabla\delta\boldsymbol{\varphi}_h dV+\int_{\partial_I B_h}[\![\delta\boldsymbol{\varphi}_h]\!]\cdot\langle\boldsymbol{\varepsilon}\left(\boldsymbol{\varphi}_h\right):\mathcal{H}\rangle\cdot\mathbf{n}^- dS+\\ \int_{\partial_I B_h}[\![\delta\boldsymbol{\varphi}_h]\!]\otimes\mathbf{n}^-:\left\langle\frac{\beta}{h_{\mathrm{s}}}\mathcal{H}\right\rangle:[\![\boldsymbol{\varphi}_h]\!]\otimes\mathbf{n}^- dS=\int_{B_h}\rho\mathbf{B}\cdot\delta\boldsymbol{\varphi}_h dV+\\ \int_{\partial_N B_h}\bar{\mathbf{T}}\cdot\delta\boldsymbol{\varphi}_h dS\quad\forall\delta\boldsymbol{\varphi}_h\in\mathrm{X}^k_{\mathrm{h}c}\end{array}\tag{61}$$

where $\mathbf{n}^-$ is the normal in the actual configuration. This expression is rewritten in the bilinear form as finding $\boldsymbol{\varphi}_h\in\mathrm{X}^k_{\mathrm{h}}$:

$$a\left(\boldsymbol{\varphi}_h-\mathbf{X},\delta\boldsymbol{\varphi}_h\right)=b\left(\delta\boldsymbol{\varphi}_h\right)\quad\forall\delta\boldsymbol{\varphi}_h\in\mathrm{X}^k_{\mathrm{hc}}\tag{62}$$

with

$$\begin{aligned}a\left(\mathbf{u}_h,\delta\boldsymbol{\varphi}_h\right)&=\int_{B_h}\nabla\mathbf{u}_h:\mathcal{H}:\nabla\delta\boldsymbol{\varphi}_h dV+\\&\quad\int_{\partial_I B_h}[\![\delta\boldsymbol{\varphi}_h]\!]\otimes\mathbf{n}^-:\left\langle\frac{\beta}{h_{\mathrm{s}}}\mathcal{H}\right\rangle:[\![\mathbf{u}_h]\!]\otimes\mathbf{n}^- dS+\\&\quad\int_{\partial_I B_h}\mathbf{n}^-\cdot\langle\mathcal{H}:\nabla\mathbf{u}_h\rangle\cdot[\![\delta\boldsymbol{\varphi}_h]\!]\,dS\end{aligned}\tag{63}$$

$$b\left(\delta\boldsymbol{\varphi}_h\right)=\int_{B_h}\rho\delta\boldsymbol{\varphi}_h\cdot\mathbf{B}dV+\int_{\partial_N B_h}\bar{\mathbf{T}}\cdot\delta\boldsymbol{\varphi}_h dS\tag{64}$$

where $\mathbf{u}_h$ can be seen as a displacement field and where we have used the symmetry of $\mathcal{H}$ ($\nabla\mathbf{u}_h:\mathcal{H}=\frac{1}{2}\nabla\mathbf{u}_h:\mathcal{H}+\frac{1}{2}\mathbf{u}_h\nabla:\mathcal{H}$). From this expression we can still demonstrate the consistency, but also the stability and we can determinate the convergence rate.

I.3. Consistency in the linear range

Consistency in the non-linear range was demonstrated in section (I.1). In the linear range this consistency is of course still verified and therefore the exact solution $\mathbf{x}$ verifies the linear relation (62). Using the linear properties of this function the consistency relation can also be

expressed by:

$$\begin{aligned} a\left(\boldsymbol{\varphi}_h - \boldsymbol{\varphi}, \delta\boldsymbol{\varphi}_h\right) &= a\left(\boldsymbol{\varphi}_h - \mathbf{X}, \delta\boldsymbol{\varphi}_h\right) - a\left(\boldsymbol{\varphi} - \mathbf{X}, \delta\boldsymbol{\varphi}_h\right) \\ &= a\left(\boldsymbol{\varphi}_h - \mathbf{x}_0, \delta\boldsymbol{\varphi}_h\right) - b\left(\delta\boldsymbol{\varphi}_h\right) = 0 \end{aligned} \tag{65}$$

I.4. Stability

Let h_e be the size of the subdomain Ω_0^e:

$$h_e = \max_{\mathrm{B}\in\Omega_0^e} \{\mathrm{diamB}\} \tag{66}$$

where B is a ball. We assume the discretization is regular:

$$\exists a > 0 \ : \qquad \tfrac{h_e}{a} \leq \min_{\mathrm{B}\ni\Omega_0^e} \{\mathrm{diamB}\} \tag{67}$$

$$h_e \to 0 \quad \text{is the only accumulation point} \tag{68}$$

Therefore, one can define the discretization size by

$$h_{\max} = \max_e h_e \tag{69}$$

In this section we assume that the Dirichlet conditions correspond to an imposed displacement equal to zero. Let us define $\mathrm{X}_\mathrm{c}^\mathrm{f}\left(B_{0h}\right)$ the constraint space:

$$\mathrm{X}_\mathrm{c}^\mathrm{f}\left(B_{0h}\right) = \left\{ \mathbf{v} \in \mathrm{X}^\mathrm{f}\left(B_{0h}\right) |_{\left[\mathbf{v}|_{\partial_D B} = 0\right]} \right\} \tag{70}$$

Let us define the norm $|||\bullet|||$: $\mathrm{X}_\mathrm{c}^\mathrm{f}\left(B_{0h}\right) \to \mathbb{R}_+$:

$$\begin{aligned} |||\mathbf{v}|||^2 &= \sum_e \left\| \sqrt{\mathcal{H}} : \nabla\mathbf{v} \right\|^2_{\mathrm{L}^2(\Omega^e)} + \sum_{\mathrm{s}\in\partial_I B_h} \left\| h_\mathrm{s}^{-\frac{1}{2}} \sqrt{\mathcal{H}} : [\![\mathbf{v}]\!] \otimes \mathbf{n}^- \right\|^2_{\mathrm{L}^2(\mathrm{s})} \\ &= \sum_e \left\| \sqrt{\mathcal{H}} : \nabla\mathbf{v} \right\|^2_{\mathrm{L}^2(\Omega^e)} + \sum_e \frac{1}{2} \left\| h_\mathrm{s}^{-\frac{1}{2}} \sqrt{\mathcal{H}} : [\![\mathbf{v}]\!] \otimes \mathbf{n}^- \right\|^2_{\mathrm{L}^2(\partial\Omega^e \cap \partial_I B_h)} \end{aligned} \tag{71}$$

Existence of $\sqrt{\mathcal{H}}$ is ensured by its symmetry properties. Contrarily to Hansbo and Costanzo [12] we introduced this term in the norm as proposed by Engel *et al.* [13] when studying plates

in linear elasticity. Expression (71) is a norm in the constraint space $\mathrm{X}_{\mathrm{c}}^{\mathrm{f}}(B_{0h})$. If right part is equal to zero, then $\nabla\mathbf{v}$ is also equal to zero. Therefore $\mathbf{v}$ has the equation of a rigid motion on each element Ω_0^e. If the right part is null then the jump is also null and the rigid motion is global. Since $\mathbf{v} \in \mathrm{X}_{\mathrm{c}}^{\mathrm{f}}(B_{0h})$ enforces strictly the Dirichlet condition $\mathbf{v} = 0$ this rigid motion is null.

Let us consider $\mathbf{v}, \quad \delta\mathbf{v} \in \mathrm{X}_{\mathrm{c}}^{\mathrm{f}}(B_{0h})$. The Cauchy-Schwartz inequality ($|\mathbf{a} : \mathbf{b}| \leq \|\mathbf{a}\| \, \|\mathbf{b}\|$) leads to:

$$\begin{aligned} \left| \int_B \nabla\mathbf{v} : \mathcal{H} : \nabla\delta\mathbf{v} dV \right| &\leq \sum_e \left| \int_{\Omega^e} \nabla\mathbf{v} : \mathcal{H} : \nabla\delta\mathbf{v} dV \right| \\ &\leq \sum_e \left\| \sqrt{\mathcal{H}} : \nabla\mathbf{v} \right\|_{\mathrm{L}^2(\Omega^e)} \left\| \sqrt{\mathcal{H}} : \nabla\delta\mathbf{v} \right\|_{\mathrm{L}^2(\Omega^e)} \end{aligned} \tag{72}$$

Moreover one has:

$$\begin{gathered} \left| \int_{\partial_I B_h} [\![\delta\mathbf{v}]\!] \otimes \mathbf{n}^- : \left\langle \tfrac{\beta}{h_{\mathrm{s}}} \mathcal{H} \right\rangle : [\![\mathbf{v}]\!] \otimes \mathbf{n}^- dS \right| = \\ \tfrac{1}{2} \left| \sum_e \int_{\partial\Omega^e \cap \partial_I B_h} [\![\delta\mathbf{v}]\!] \otimes \mathbf{n}^- : \left\langle \tfrac{\beta}{h_{\mathrm{s}}} \mathcal{H} \right\rangle : [\![\mathbf{v}]\!] \otimes \mathbf{n}^- dS \right| \leq \\ \tfrac{1}{2}\beta \sum_e \left\| h_{\mathrm{s}}^{-\frac{1}{2}} \sqrt{\mathcal{H}} : [\![\mathbf{v}]\!] \otimes \mathbf{n}^- \right\|_{\mathrm{L}^2(\Omega^e \cap \partial_I B_h)} \left\| h_{\mathrm{s}}^{-\frac{1}{2}} \sqrt{\mathcal{H}} : [\![\delta\mathbf{v}]\!] \otimes \mathbf{n}^- \right\|_{\mathrm{L}^2(\partial\Omega^e \cap \partial_I B_h)} \end{gathered} \tag{73}$$

and:

$$\begin{gathered} \left| \int_{\partial_I B_h} \mathbf{n}^- \cdot \langle \mathcal{H} : \nabla\mathbf{v} \rangle \cdot [\![\delta\mathbf{v}]\!] \, dS \right| = \tfrac{1}{2} \left| \sum_e \int_{\partial\Omega^e \cap \partial_I B_h} \mathbf{n}^- \cdot \langle \mathcal{H} : \nabla\mathbf{v} \rangle \cdot [\![\delta\mathbf{v}]\!] \, dS \right| \leq \\ \tfrac{1}{2} \sum_e \left\| h_{\mathrm{s}}^{\frac{1}{2}} \sqrt{\mathcal{H}} : \langle \nabla\mathbf{v} \rangle \right\|_{\mathrm{L}^2(\partial\Omega^e \cap \partial_I B_h)} \left\| h_{\mathrm{s}}^{-\frac{1}{2}} \sqrt{\mathcal{H}} : [\![\delta\mathbf{v}]\!] \otimes \mathbf{n}^- \right\|_{\mathrm{L}^2(\partial\Omega^e \cap \partial_I B_h)} \leq \\ \sum_e \left\| h_{\mathrm{s}}^{\frac{1}{2}} \sqrt{\mathcal{H}} : \nabla\mathbf{v} \right\|_{\mathrm{L}^2(\partial\Omega^e \cap \partial_I B_h)} \left\| h_{\mathrm{s}}^{-\frac{1}{2}} \sqrt{\mathcal{H}} : [\![\delta\mathbf{v}]\!] \otimes \mathbf{n}^- \right\|_{\mathrm{L}^2(\partial\Omega^e \cap \partial_I B_h)} \leq \\ C^k \sum_e \left\| \sqrt{\mathcal{H}} : \nabla\mathbf{v} \right\|_{\mathrm{L}^2(\Omega^e)} \left\| h_{\mathrm{s}}^{-\frac{1}{2}} \sqrt{\mathcal{H}} : [\![\delta\mathbf{v}]\!] \otimes \mathbf{n}^- \right\|_{\mathrm{L}^2(\partial\Omega^e \cap \partial_I B_h)} \end{gathered} \tag{74}$$

where we have used the property $\|\langle \bullet \rangle\|_{\mathrm{L}^2(\mathrm{s})} \leq \|\bullet^-\|_{\mathrm{L}^2(\mathrm{s})} + \|\bullet^+\|_{\mathrm{L}^2(\mathrm{s})}$ and the scaling properties.[‡]

[‡]Hansbo et al have shown [12] that for an element e one has $h_{\mathrm{s}} \|\nabla\mathbf{v}\|^2_{\mathrm{L}^2(\partial\Omega^e)} \leq C^k \|\nabla\mathbf{v}\|^2_{\mathrm{L}^2(\Omega^e)}$ with $C^k > 0$

Relations (72), (73) and (74) lead to two interesting results. First result is an upper bound of the bilinear form. From relation (63), the triangular inequality leads to:

$$\begin{aligned} |a(\mathbf{v},\delta\mathbf{v})| &\leq \left|\int_{B_h} \nabla\mathbf{v} : \mathcal{H} : \nabla\delta\mathbf{v} dV\right| + \left|\int_{\partial_I B_h} [\![\delta\mathbf{v}]\!]\otimes\mathbf{n}^- : \left\langle \frac{\beta}{h_\mathrm{s}}\mathcal{H}\right\rangle : [\![\mathbf{v}]\!]\otimes\mathbf{n}^- dS\right| + \\ &\quad \left|\int_{\partial_I B_h} \mathbf{n}^-\cdot\langle\mathcal{H}:\nabla\mathbf{v}\rangle\cdot[\![\delta\mathbf{v}]\!]\, dS\right| \end{aligned} \tag{75}$$

By using relations (72), (73) and (74), this last expression is rewritten as:

$$\begin{aligned} |a(\mathbf{v},\delta\mathbf{v})| &\leq \sum_e \left\|\sqrt{\mathcal{H}}:\nabla\mathbf{v}\right\|_{\mathrm{L}^2(\Omega^e)} \left\|\sqrt{\mathcal{H}}:\nabla\delta\mathbf{v}\right\|_{\mathrm{L}^2(\Omega^e)} + \\ &\quad \frac{1}{2}\beta\sum_e \left\|h_\mathrm{s}^{-\frac{1}{2}}\sqrt{\mathcal{H}}:[\![\mathbf{v}]\!]\otimes\mathbf{n}^-\right\|_{\mathrm{L}^2(\partial\Omega^e\cap\partial_I B_h)} \left\|h_\mathrm{s}^{-\frac{1}{2}}\sqrt{\mathcal{H}}:[\![\delta\mathbf{v}]\!]\otimes\mathbf{n}^-\right\|_{\mathrm{L}^2(\partial\Omega^e\cap\partial_I B_h)} \\ &\quad + C^k\sum_e \left\|\sqrt{\mathcal{H}}:\nabla\mathbf{v}\right\|_{\mathrm{L}^2(\Omega^e)} \left\|h_\mathrm{s}^{-\frac{1}{2}}\sqrt{\mathcal{H}}:[\![\delta\mathbf{v}]\!]\otimes\mathbf{n}^-\right\|_{\mathrm{L}^2(\partial\Omega^e\cap\partial_I B_h)} \\ &\leq C_1(\beta)\sum_e \left\|\sqrt{\mathcal{H}}:\nabla\mathbf{v}\right\|_{\mathrm{L}^2(\Omega^e)} \left\|\sqrt{\mathcal{H}}:\nabla\delta\mathbf{v}\right\|_{\mathrm{L}^2(\Omega^e)} + \\ &\quad C_1(\beta)\sum_e \left\|\frac{\sqrt{\mathcal{H}}:[\![\mathbf{v}]\!]\otimes\mathbf{n}^-}{\sqrt{2h_\mathrm{s}}}\right\|_{\mathrm{L}^2(\partial\Omega^e\cap\partial_I B_h)} \left\|\frac{\sqrt{\mathcal{H}}:[\![\delta\mathbf{v}]\!]\otimes\mathbf{n}^-}{\sqrt{2h_\mathrm{s}}}\right\|_{\mathrm{L}^2(\partial\Omega^e\cap\partial_I B_h)} \\ &\quad + C_1(\beta)\sum_e \left\|\sqrt{\mathcal{H}}:\nabla\mathbf{v}\right\|_{\mathrm{L}^2(\Omega^e)} \left\|\sqrt{\frac{1}{2h_\mathrm{s}}}\sqrt{\mathcal{H}}:[\![\delta\mathbf{v}]\!]\otimes\mathbf{n}^-\right\|_{\mathrm{L}^2(\partial\Omega^e\cap\partial_I B_h)} + \\ &\quad C_1(\beta)\sum_e \left\|\sqrt{\mathcal{H}}:\nabla\delta\mathbf{v}\right\|_{\mathrm{L}^2(\Omega^e)} \left\|\sqrt{\frac{1}{2h_\mathrm{s}}}\sqrt{\mathcal{H}}:[\![\mathbf{v}]\!]\otimes\mathbf{n}^-\right\|_{\mathrm{L}^2(\partial\Omega^e\cap\partial_I B_h)} \end{aligned} \tag{76}$$

with $C_1(\beta) = \max\left(1,\beta,\sqrt{2}C^k\right)$. The previous relation is rewritten:

$$\begin{aligned} \frac{|a(\mathbf{v},\delta\mathbf{v})|}{C_1(\beta)} &\leq \sum_e \left[\left\|\sqrt{\mathcal{H}}:\nabla\mathbf{v}\right\|_{\mathrm{L}^2(\Omega^e)} + \left\|\frac{\sqrt{\mathcal{H}}:[\![\mathbf{v}]\!]\otimes\mathbf{n}^-}{\sqrt{2h_\mathrm{s}}}\right\|_{\mathrm{L}^2(\partial\Omega^e\cap\partial_I B_h)}\right] \\ &\quad \times\left[\left\|\sqrt{\mathcal{H}}:\nabla\delta\mathbf{v}\right\|_{\mathrm{L}^2(\Omega^e)} + \left\|\frac{\sqrt{\mathcal{H}}:[\![\delta\mathbf{v}]\!]\otimes\mathbf{n}^-}{\sqrt{2h_\mathrm{s}}}\right\|_{\mathrm{L}^2(\partial\Omega^e\cap\partial_I B_h)}\right] \end{aligned} \tag{77}$$

The Cauchy-Schwartz inequality ($|\sum_i a_i b_i| \leq \sqrt{\sum_i a_i^2 \sum_j b_j^2}$) and the property $2ab \leq a^2+b^2$

---

independent of the element geometry and with $h_\mathrm{s} = \frac{|\Omega^e|}{|\partial\Omega^e|}$. Constant $C^k = \sup_{\mathbf{v}\in\mathbb{P}^k(\Omega_0^e)} \frac{|\Omega^e|\int_\mathrm{s}\{\nabla\mathbf{v}:\nabla\mathbf{v}\}dS}{|\mathrm{s}|\int_{\Omega^e}\{\nabla\mathbf{v}:\nabla\mathbf{v}\}dV}$ depends only on the polynomial degree k.

lead to:

$$\begin{aligned}
\frac{|a(\mathbf{v},\delta\mathbf{v})|^2}{[C_1(\beta)]^2} &\leq \sum_e \left[\left\| \sqrt{\mathcal{H}} : \nabla\mathbf{v} \right\|_{\mathrm{L}^2(\Omega^e)} + \left\| (2h_{\mathrm{s}})^{-\frac{1}{2}} \sqrt{\mathcal{H}} : [\![\mathbf{v}]\!] \otimes \mathbf{n}^- \right\|_{\mathrm{L}^2(\partial\Omega^e \cap \partial_I B_h)} \right]^2 \\
&\quad \sum_{e'} \left[\left\| \sqrt{\mathcal{H}} : \nabla\delta\mathbf{v} \right\|_{\mathrm{L}^2\left(\Omega^{e'}\right)} + \left\| (2h_{\mathrm{s}})^{-\frac{1}{2}} \sqrt{\mathcal{H}} : [\![\delta\mathbf{v}]\!] \otimes \mathbf{n}^- \right\|_{\mathrm{L}^2\left(\partial\Omega^{e'} \cap \partial_I B_h\right)} \right]^2 \\
&\leq 4 \sum_e \left[\left\| \sqrt{\mathcal{H}} : \nabla\mathbf{v} \right\|^2_{\mathrm{L}^2(\Omega^e)} + \frac{1}{2} \left\| h_{\mathrm{s}}^{-\frac{1}{2}} \sqrt{\mathcal{H}} : [\![\mathbf{v}]\!] \otimes \mathbf{n}^- \right\|^2_{\mathrm{L}^2(\partial\Omega^e \cap \partial_I B_h)} \right] \\
&\quad \sum_{e'} \left[\left\| \sqrt{\mathcal{H}} : \nabla\delta\mathbf{v} \right\|^2_{\mathrm{L}^2\left(\Omega^{e'}\right)} + \frac{1}{2} \left\| h_{\mathrm{s}}^{-\frac{1}{2}} \sqrt{\mathcal{H}} : [\![\delta\mathbf{v}]\!] \otimes \mathbf{n}^- \right\|^2_{\mathrm{L}^2\left(\partial\Omega^{e'} \cap \partial_I B_h\right)} \right] \qquad (78)
\end{aligned}$$

Introducoing the factor 4 in C_1, and using (71), one has the upper bound relation:

$$|a(\mathbf{v},\delta\mathbf{v})| \leq C_1(\beta) \, |||\mathbf{v}||| \, |||\delta\mathbf{v}||| \quad \forall \mathbf{v}, \delta\mathbf{v} \in \mathrm{X}^{\mathrm{f}}_{\mathrm{c}}(B_{0h}) \qquad (79)$$

where $C_1(\beta)$ is independent of the size of the mesh.

Second result corresponds to a lower bound of the bilinear norm. From relation (63), one has:

$$\begin{aligned}
a(\mathbf{v},\mathbf{v}) &= \sum_e \left\| \sqrt{\mathcal{H}} : \nabla\mathbf{v} \right\|^2_{\mathrm{L}^2(\Omega^e)} + \beta \sum_{\mathrm{s} \in \partial_I B_h} \left\| h_{\mathrm{s}}^{-\frac{1}{2}} \sqrt{\mathcal{H}} : [\![\mathbf{v}]\!] \otimes \mathbf{n}^- \right\|^2_{\mathrm{L}^2(\mathrm{s})} + \\
&\quad \int_{\partial_I B_h} \mathbf{n}^- \cdot \langle \mathcal{H} : \nabla\mathbf{v} \rangle \cdot [\![\mathbf{v}]\!] \, dS \\
&\geq \sum_e \left\| \sqrt{\mathcal{H}} : \boldsymbol{\varepsilon} \right\|^2_{\mathrm{L}^2(\Omega^e)} + \frac{\beta}{2} \sum_e \left\| h_{\mathrm{s}}^{-\frac{1}{2}} \sqrt{\mathcal{H}} : [\![\mathbf{x}_{\mathrm{h}}]\!] \otimes \mathbf{n}^- \right\|^2_{\mathrm{L}^2(\partial\Omega^e \cap \partial_I B_h)} \\
&\quad - \left| \int_{\partial_I B_h} \mathbf{n}^- \cdot \langle \mathcal{H} : \nabla\mathbf{v} \rangle \cdot [\![\mathbf{v}]\!] \, dS \right| \quad \forall \mathbf{v} \in \mathrm{X}^{\mathrm{f}}_{\mathrm{c}}(B_{0h}) \qquad (80)
\end{aligned}$$

Using (74) leads to:

$$\begin{aligned}
a(\mathbf{v},\mathbf{v}) &\geq \sum_e \left\| \sqrt{\mathcal{H}} : \nabla\mathbf{v} \right\|^2_{\mathrm{L}^2(\Omega^e)} + \frac{\beta}{2} \sum_e \left\| h_{\mathrm{s}}^{-\frac{1}{2}} \sqrt{\mathcal{H}} : [\![\mathbf{v}]\!] \otimes \mathbf{n}^- \right\|^2_{\mathrm{L}^2(\partial\Omega^e \cap \partial_I B_h)} - \\
&\quad C^k \sum_e \left\| \sqrt{\mathcal{H}} : \nabla\mathbf{v} \right\|_{\mathrm{L}^2(\Omega^e)} \left\| h_{\mathrm{s}}^{-\frac{1}{2}} \sqrt{\mathcal{H}} : [\![\mathbf{v}]\!] \otimes \mathbf{n}^- \right\|_{\mathrm{L}^2(\partial\Omega^e \cap \partial_I B_h)} \qquad (81)
\end{aligned}$$

The ε-inequality[§], this last relation is rewritten

$$\begin{aligned} a(\mathbf{v},\mathbf{v}) \quad &\geq \quad \sum_e [1-\varepsilon] \left\| \sqrt{\mathcal{H}} : \nabla \mathbf{v} \right\|^2_{\mathrm{L}^2(\Omega^e)} + \\ &\left[\frac{\beta}{2} - \frac{{C^k}^2}{4\varepsilon} \right] \sum_e \left\| h_{\mathrm{s}}^{-\frac{1}{2}} \sqrt{\mathcal{H}} : [\![\mathbf{v}]\!] \otimes \mathbf{n}^- \right\|^2_{\mathrm{L}^2(\partial\Omega^e \cap \partial_I B_h)} \end{aligned} \tag{82}$$

Let $C_2(\beta) = \min\left(1-\varepsilon, \beta - \frac{{C^k}^2}{2\varepsilon}\right)$ that is positive providing $\beta \geq \frac{{C^k}^2}{2\varepsilon}$ and $\varepsilon < 1$. Therefore, using (71), relation (82) becomes:

$$a(\mathbf{v},\mathbf{v}) \quad \geq \quad C_2(\beta) \left|\left|\left| \mathbf{v} \right|\right|\right|^2 \quad \forall \mathbf{v} \in \mathrm{X}^{\mathrm{f}}_{\mathrm{c}}(B_{0h}) \tag{83}$$

Let us rewrite this relation for the finite approximation. Since $\boldsymbol{\varphi}_h - \mathbf{X} \in \mathrm{X}^k_{\mathrm{hc}} \subset \mathrm{X}^{\mathrm{f}}_{\mathrm{c}}(B_{0h})$ since the Dirichlet conditions were enforced strictly, one has:

$$a(\boldsymbol{\varphi}_h - \mathbf{X}, \boldsymbol{\varphi}_h - \mathbf{X}) \quad \geq \quad C_2(\beta) \left|\left|\left| \boldsymbol{\varphi}_h - \mathbf{X} \right|\right|\right|^2 \quad \forall \boldsymbol{\varphi}_h - \mathbf{X} \in \mathrm{X}^k_{\mathrm{hc}} \tag{84}$$

This last expression demonstrates the stability of the method, since the energy norm is bounded. Let us remark that C^k depends only on the polynomial degree.

I.5. Convergence

If $\boldsymbol{\varphi} \in \mathrm{X}^{\mathrm{f}}(B_{0h})$ is the exact solution of the problem, we can define $\boldsymbol{\varphi}^k$ the interpolation in $\mathrm{X}^k_{\mathrm{h}}$ by:

$$\int_{B_h} \left[\boldsymbol{\varphi} - \boldsymbol{\varphi}^k\right] \cdot \delta\mathbf{v} dV = 0 \quad \forall \delta\mathbf{v} \in \mathrm{X}^k_{\mathrm{h}} \tag{85}$$

Let us define the error $\mathbf{e} = \boldsymbol{\varphi}_h - \boldsymbol{\varphi} \in \mathrm{X}^{\mathrm{f}}_{\mathrm{c}}(B_{0h})$ (where we assume the imposed displacement on Dirichlet boundary equal to zero and strictly enforced) and the error of the interpolated solution $\mathbf{e}^k = \boldsymbol{\varphi}_h - \boldsymbol{\varphi}^k \in \mathrm{X}^k_{\mathrm{hc}} \subset \mathrm{X}^{\mathrm{f}}_{\mathrm{c}}(B_{0h})$. Since the bilinear form (63, 64) is by definition

[§] $\forall \epsilon > 0 : |ab| \leq \frac{\epsilon}{2} a^2 + \frac{1}{2\epsilon} b^2$ or $\forall \epsilon > 0 : |ab| \leq \epsilon a^2 + \frac{1}{4\epsilon} b^2$.

linear, using (79) and (84) yields:

$$\begin{aligned} C_2 \left|\left|\left|\mathbf{e}^k\right|\right|\right|^2 &\leq a\left(\boldsymbol{\varphi}_h - \boldsymbol{\varphi}^k, \boldsymbol{\varphi}_h - \boldsymbol{\varphi}^k\right) = a\left(\boldsymbol{\varphi}_h - \boldsymbol{\varphi}, \boldsymbol{\varphi}_h - \boldsymbol{\varphi}^k\right) + a\left(\boldsymbol{\varphi} - \boldsymbol{\varphi}^k, \boldsymbol{\varphi}_h - \boldsymbol{\varphi}^k\right) \\ &\leq C_1 \left|\left|\left|\boldsymbol{\varphi} - \boldsymbol{\varphi}^k\right|\right|\right| \left|\left|\left|\boldsymbol{\varphi}_h - \boldsymbol{\varphi}^k\right|\right|\right| = C_1 \left|\left|\left|\boldsymbol{\varphi} - \boldsymbol{\varphi}^k\right|\right|\right| \left|\left|\left|\mathbf{e}^k\right|\right|\right| \end{aligned} \tag{86}$$

where we have used (65) to annihilate the term $a\left(\boldsymbol{\varphi}_h - \boldsymbol{\varphi}, \boldsymbol{\varphi}_h - \boldsymbol{\varphi}^k\right)$. Now we have to estimate the right part of this equation.

First term of the definition of norm (71) can be evaluated:

$$\left\|\sqrt{\mathcal{H}} : \nabla\left[\boldsymbol{\varphi} - \boldsymbol{\varphi}^k\right]\right\|^2_{\mathrm{L}^2(\Omega^e)} \leq c C_i h^{2k}_{\max} \left\|\boldsymbol{\varphi} - \mathbf{X}\right\|^2_{\mathrm{H}^{k+1}(\Omega^e)} \tag{87}$$

where we have used successively the positive definiteness of $\mathcal{H}$[¶], the definition of the norm in the Sobolev space ($\|\nabla\boldsymbol{\varphi}\|_{\mathrm{H}^0(\Omega^e)} \leq \|\boldsymbol{\varphi}\|_{\mathrm{H}^1(\Omega^e)}$), the basic error estimates of interpolation theory[‖], and the relation $h_e < h_{\max}$. Moreover, one has:

$$\begin{aligned} \left\|h_{\mathrm{s}}^{-\frac{1}{2}}\sqrt{\mathcal{H}} : [\![\boldsymbol{\varphi} - \boldsymbol{\varphi}^k]\!] \otimes \mathbf{n}^-\right\|^2_{\mathrm{L}^2(\mathrm{s}\in\partial_I B_h)} &\leq C \left\|h_e^{-\frac{1}{2}}\sqrt{\mathcal{H}} : [\![\boldsymbol{\varphi} - \boldsymbol{\varphi}^k]\!] \otimes \mathbf{n}^-\right\|^2_{\mathrm{L}^2(\partial\Omega^e)} \\ &\leq c C_T \left[\frac{\left\|\boldsymbol{\varphi} - \boldsymbol{\varphi}^k\right\|^2_{\mathrm{L}^2(\Omega^e)}}{h^2_{\mathrm{e}}} + \left\|\nabla\left[\boldsymbol{\varphi} - \boldsymbol{\varphi}^k\right]\right\|^2_{\mathrm{L}^2(\Omega^e)}\right] \\ &\leq c C_T \left[\frac{\left\|\boldsymbol{\varphi} - \boldsymbol{\varphi}^k\right\|^2_{\mathrm{L}^2(\Omega^e)}}{h^2_{\mathrm{e}}} + \left\|\boldsymbol{\varphi} - \boldsymbol{\varphi}^k\right\|^2_{\mathrm{H}^1(\Omega^e)}\right] \\ &\leq C'_T \left\|\boldsymbol{\varphi} - \boldsymbol{\varphi}^k\right\|^2_{\mathrm{H}^1(\Omega^e)} \\ &\leq C'_i h^{2k}_e \left\|\boldsymbol{\varphi} - \boldsymbol{\varphi}^k\right\|^2_{\mathrm{H}^{k+1}(\Omega^e)} \\ &\leq C'_i h^{2k}_{\max} \left\|\boldsymbol{\varphi} - \mathbf{X}\right\|^2_{\mathrm{H}^{k+1}(\Omega^e)} \end{aligned} \tag{88}$$

where we use successively the fact that for one given element h_{s} is proportional to h_e,

[¶] $\exists c > 0 : \mathbf{a} : \mathcal{H} : \mathbf{a} \leq c\mathbf{a} : \mathbf{a}$.

[‖] Given a function $\boldsymbol{\varphi} \in \mathrm{H}^{k+1}\left(\Omega^e_0\right)$, then $\forall \boldsymbol{\varphi}^k \in \mathbb{P}^k\left(\Omega^e_0\right)$ interpolating $\boldsymbol{\varphi}$ in Ω^e[26]: $\left\|\boldsymbol{\varphi} - \boldsymbol{\varphi}^k\right\|_{\mathrm{H}^q(\Omega^e)} \leq C_i h_e^{k+1-q} \left\|\boldsymbol{\varphi}\right\|_{\mathrm{H}^{k+1}(\Omega^e)} \forall 0 \leq q \leq k+1$, with C_i independent of h_e, the size of Ω^h_0.

the positive definiteness of $\mathcal{H}$, the trace inequality**, the definition of Sobolev spaces (*i.e.* $\|\nabla \mathbf{x}\|_{\mathrm{H}^0(\Omega^e)} \leq \|\mathbf{x}\|_{\mathrm{H}^1(\Omega^e)}$), the inverse inequality†† and the interpolant norm. Therefore, combining (87) and (88) leads to:

$$\left|\left|\left|\boldsymbol{\varphi} - \boldsymbol{\varphi}^k\right|\right|\right|^2 \leq C_3 \sum_e h_{\max}^{2k} \|\boldsymbol{\varphi} - \mathbf{X}\|^2_{\mathrm{H}^{k+1}(\Omega^e)} \tag{89}$$

where $C_3 > 0$ does not depends on $\mathrm{h}_{\max}$.

Finally, combining relations (86) and (89) one has:

$$\left|\left|\left|\mathbf{e}^k\right|\right|\right| \leq C_4 h_{\max}^k \|\boldsymbol{\varphi} - \mathbf{X}\|_{\mathrm{H}^{k+1}(B_h)} \tag{90}$$

where $C_4 > 0$. This expression demonstrates that the order of convergence is the order of the polynomial approximation providing $\boldsymbol{\varphi} \in \mathrm{H}^{k+1}(B_h)$. Since we dropped the symmetric term we cannnot reach a convergence rate of $k+1$ in the L^2-norm [27]. But the last relation demonstrates that we have at least a convergence rate of k in the L^2-norm.

II. STIFFNESS MATRIX

In this section we provide an approximation of the stiffness matrix resulting from the interface forces (50). When analyzing this expression it is clear that the forces of the interface element depend on the stresses (and on the material moduli) of the two adjacent tetrahedra. Therefore the stiffness matrix involves all the degrees of freedom of the two adjacent elements and not only those comprised by the interface element itself. This increases the complexity of the implementation and—possibly—the bandwidth of the assembled global system of equations. Taking into consideration that for stable values of β the displacement jumps are small, as shown

**$\forall \mathbf{v} \in \mathrm{H}^1(\Omega^e) \quad \exists C_T > 0 : \|\mathbf{v}\|^2_{\mathrm{L}^2(\partial\Omega^e)} \leq \frac{C_T}{h_e} \|\mathbf{v}\|^2_{\mathrm{L}^2(\Omega^e)} + C_T h_e \|\nabla \mathbf{v}\|^2_{\mathrm{L}^2(\Omega^e)}$ [26].

††$\forall m < l \quad \exists C_I > 0 : \quad \|\mathbf{v}\|_{\mathrm{H}^m(\Omega^e)} \leq C_I h_e^{l-m} \|\mathbf{v}\|_{\mathrm{H}^l(\Omega^e)}$ [26].

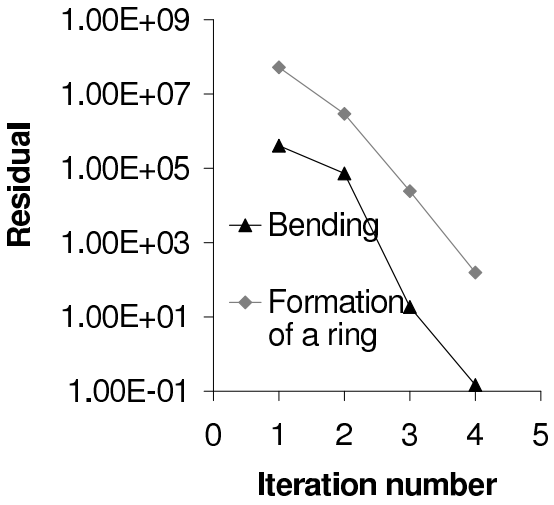

Figure 15. Residual norm vs number of Newton-Raphson iterations in the solution of the nonlinear system of equations for problems in Sections 4.2 and 4.3

in the application examples, we propose to take into account only the geometric part (due to the jump) of the stiffness matrix. We will show that the convergence of the Newton-Raphson iterations is not affected by this simplification whereas it provides considerable simplification of the implementation and considerable computational savings.

The geometric part of the stiffness matrix results from the jump in the last term of relation (50). A straightforward derivation leads to:

$$\mathbf{K}^{\pm\pm}_{ab\ ij} \quad = \quad \frac{\partial \mathbf{f}^{I\pm}_{a\ i}}{\partial \mathbf{x}^{\pm}_{b\ j}} = \pm \int_{\partial_I B_{0h}} \left\langle \frac{\beta}{h_{\mathrm{s}}} \bar{\mathbb{C}} \right\rangle_{iJjL} N_a \mathbf{N}^-_J N_b \mathbf{N}^-_L dS \tag{91}$$

with a plus sign for the combinations $\xi + \mu +$ and $\xi - \mu -$ and with a minus sign for other combinations.

Figure 15 illustrates the convergence of the Newton-Raphson iterations when considering the bending in large deformation of the beam (discretization 2, stabilization parameter $\beta = 10$)

and when considering the formation of a ring. The evolution of the residual shown corresponds to a representative load step at the end of the simulation. It can be observed that despite the inconsistency of the stiffness matrix the convergence rate appears to be close to quadratic. It can therefore be concluded that the approximate stiffness of the interface elements proposed in equation (91) does not affect the solution of the system of nonlinear equations while it is significantly advantageous for the reasons alluded to above.

ACKNOWLEDGEMENTS

This research was supported by the U.S. Army through the Institute for Soldier Nanotechnologies, under Contract DAAD-19-02-D-0002 with the U.S. Army Research Office. The content does not necessarily reflect the position of the Government, and no official endorsement should be inferred.

REFERENCES

1. Nitsche JA. Uber ein variationsprinzip zur Lösung Dirichlet-Problemen bei Verwendung von Teilräumen, die keinen Randbedingungen uneworfen sind. *Abhandlungen aus dem Mathematischen Seminar der Universität Hamburg* 1971; **36**:9–15.
2. Reed WH and Hill TR. Triangular mesh methods for the neutron transport equation. Technical Report LA-UR-73-479, Los Alamos Scientific Laboratory, 1973.
3. Cockburn B. Discontinuous Galerkin methods for convection-dominated problems. In Quaterroni A, editor, *High-Order Methods for Computational Physics*, volume 11, pages 69–213, 2003. Lecture Notes in Computational Sciences and Engineering.
4. Cockburn B. Discontinuous Galerkin methods. *Zeitschrift fuer Angewandte Mathematik und Mechanik* 2003; **83**(11):731–754.
5. Cockburn B, Hou S, and Shu CW. TVB Range-Kutta local projection discontinuous Galerkin finite element method for conservation laws IV: The multidimensional case. *Mathematics of Computation* 1990; **54**:545–581.

6. Palaniappan J, Haber RB, and Jerrard RL. A spacetime discontinuous Galerkin method for scalar conservation laws. *Computer Methods in Applied Mechanics and Engineering* 2004; **193**:3607–3631.
7. Bassi F and Rebay S. A high-order accurate discontinuous finite element method for the numerical solution of the compressible Navier-Stokes equations. *Journal of Computational Physics* 1997; **131**:267–279.
8. Cockburn B and Shu CW. The local discontinuous Galerkin method for time dependant convection-diffusion systems. *SIAM Journal of Numerical Analysis* 1998; **36**(6):2440–2483.
9. Brezzi F, Manzini G, Marini D, Pietra P, and Russo A. Discontinuous Galerkin approximations for elliptic problems. *Numerical Methods for Partial Differential Equations* 2000; **16**(4):365–378.
10. Kim KY. Mixed finite volume method for nonlinear elliptic problems. *Numerical Methods for Partial Differential Equations* 2005; **21**:791–809.
11. Lew A, Neff P, Sulsky D, and Ortiz M. Optimal BV estimates for a discontinuous Galerkin method for linear elasticity. *Applied Mathematics Research eXpress* 2004; **3**:73–106.
12. Hansbo P and Larson MG. Discontinuous Galerkin methods for incompressible and nearly incompressible elasticity by Nitsche's method. *Computer Methods in Applied Mechanics and Engineering* 2002; **191**:1895–1908.
13. Engel G, Garikipati K, Hughes TJR, Larson MG, Mazzei L, and Taylor RL. Continuous/discontinuous finite element approximations of fourth-order elliptic problems in structural and continuum mechanics with applications to thin beams and plates. *Computer Methods in Applied Mechanics and Engineering* 2002; **191**:3669–3750.
14. Huang H and Costanzo F. On the use of space-tim finite elements in the solution of elasto-dynamics problems with strain discontinuities. *Computer Methods in Applied Mechanics and Engineering* 2002; **191**:5315–5343.
15. Costanzo F and Huang H. Proof of unconditional stability for a single field discontinuous Galerkin finite element formulation for linear elasto-dynamics. *Computer Methods in Applied Mechanics and Engineering* 2004; **195**:in Press.
16. Bonelli A, Bursi OS, and Mancuso M. Explicit predictor-multicorrector time discontinuous galerkin methods for non-linear dynamics. *Journal of Sound and Vibration* 2002; **256**(4):695–724.
17. Chien CC, Yang CS, and Tang JH. Three-dimensional transient elastocdynamic analysis by a space and time-discontinuous Galerkin finite element method. *Finite Elements in Analysis and Design* 2003; **39**:561–580.
18. Alberty J and Cartensen C. Discontinuous Galerkin time discretization in elastoplasticity: Motivation,

numerical algorithms, and applications. *Computer Methods in Applied Mechanics and Engineering* 2002; **191**:4949–4968.

19. Mergheim J, Kuhl E, and Steinmann P. A hybrid discontinuous Galerkin/interface method for the computational modelling of failure. *Communication in Numerical Method in Engeneering* 2004; **20**:511–519.
20. Zienkiewicz OC, Taylor RL, Sherwin SJ, and Peiró J. On discontinuous Galerkin methods. *International Journal of Numerical Methods in Engineering* 2003; **58**:1119–1148.
21. Marsden J. E. and Hughes T. J. R. *Mathematical foundations of elasticity*. Dover Publications, 1993.
22. Fraijs de Veubeke BM. *Diffusion des inconnues hyperstatiques dans les voilures à longerons couplés*, volume 24 of *Bulletins du Service Technique de L'Aéronautique*. Imprimerie Marcel Hayez, Bruxelles, Belgium, 1951.
23. Hu HC. On some variational methods on the theory of elasticity and theory of plasticity. *Scientia Sinica* 1955; **4**:33–54.
24. Washizu K. On the variational principles of elasticity and plasticity. Technical Report 25-18, Aeroelastic and Structures Research Laboratory, Massachusetts Institute of Technology, Cambridge, USA, 1955.
25. Felipa CA. On the original publication of the general canonical functional of linear elasticity. *Journal of Applied Mechanics* 2000; **67**(1):217–219.
26. Ciarlet PG. *The Finite Element Method for Elliptic Problems*. North-Holland, 1978.
27. Larson MG and Niklasson AJ. Analysis of a family of dicontinuous galerkin methods for elliptic problems: The one dimensional case. *Numerische Mathematik* 2004; **99**:113–130.
28. Ortiz M. and Pandolfi A. Finite-deformation irreversible cohesive elements for three-dimensional crack-propagation analysis. *International Journal of Numerical Methods in Engineering* 1999; **44**:1267–1282.

